Final scientific report of OTKA-EraChemistry NN 107170 project entitled

Dry reforming – from understanding the elementary steps to better catalysts

Department of Surface Chemistry and Catalysis, Institute for Energy Security and Environmental Safety, Centre for Energy Research, Hungarian Academy of Sciences

Project number: NN107170 OTKA-EraChemistry
Funding period: from July 1, 2012 to December 31, 2016 (the original 36 month-period was prolonged)
Co-operating research groups's leaders:
Prof. Dr. J. A. Lercher, Technical University of Munich (project coordinator)
Prof. Dr. G. Rupprechter, Technical University of Vienna
Prof. L. Guczi†/Dr. A. Horvath, Centre for Energy Research of HAS, Budapest

1. Introduction

1.1. Scientific background and the general approach

Carbon dioxide reforming, or dry reforming of methane (DRM: $CH_4 + CO_2 \rightleftharpoons 2\ CO + 2\ H_2$) is a target reaction of high importance in CO_2-rich natural gas or biogas conversion. Although a few pilot plants have already been working worldwide under dry reforming or – combined with steam –, bi-reforming conditions,[1] there is still much to improve or even understand at the level of basic research. Depending on the reaction parameters, several side reactions may simultaneously proceed, influencing the final H_2/CO ratio (the most plausible one is the water-gas shift reaction[2]).

Concerning the reaction mechanism, the general view is that methane dissociates on the metal surface,[3,4] and CO_2 is activated on the support,[5,6] at the metal-support interface[7,8] or even on the metal surface,[6,9] depending on the reaction conditions, type of support and active metal.[10,11] In the next step, the surface CH_x fragments (x=0-3) react with active O or OH species and form a CH_xO_{surf} intermediate that after decomposition produces CO and H_2 products.[12,13,14] The suggested rate-determining steps vary with the catalyst system and reaction conditions.[15] Ni-based catalysts are probably the best choice as cost issues matter (noble metals are effective but very expensive). The hardest problem is the coke formation to tackle with under the harsh, oxygen lean reaction conditions (low CO_2 or water concentration) that usually cause fast deactivation of Ni.[16,17,18] Surprisingly, sometimes significant coke deposits can still let the catalyst work.[19,20,21,22] This is why the amount of deposited coke cannot be simply correlated with the catalytic performance and actually there is no straightforward relationship between the quantity of carbon deposition and the activity. According to Efstathiou and his co-workers,[23,24,25] we can distinguish active and inactive carbon. Inactive carbon deposits grow to graphite layers and carbon whiskers, while the active surface carbon (C_s) react with oxygen containing surface species (O_s or OH_s) and form CO desorbing into the gas phase. We should point out that only Steady State Transient Kinetic Analysis (SSITKA) is able to measure the – usually very low – surface coverage of active carbon that truly participates in the formation of CO by using labeled carbon dioxide or methane.

Reducible supports such as CeO_2 with high oxygen mobility,[19] basic supports enhancing the CO_2 adsorption/activation step[4,10,26,27] or addition of alkaline (K, CaO) promoters to the support[5,6,28,29]

may help to diminish coke formation, because carbonates formed by CO_2 adsorption at the metal-support perimeter sites are considered as scavengers of carbon.[6]

Among alkali promoters, the effect of potassium or sodium promotion was studied mostly in methanation reaction.[30,31,32] As for dry reforming specifically, it was declared that oxides of Na, K, Mg, and Ca markedly suppress the carbon deposition via the decrease of CH_4 decomposition ability of nickel. However, the positive effect highly depended on the composition of the catalyst and the preparation method.[20,28,29,33,34]

The above short literature summary will help to understand and follow our approach how to generate effective catalysts prepared from the same constituents and how to understand the elementary steps occurring during the reaction. A collaborative research was done among the Technische Universität Wien (TUW) and the Technische Universität München (TUM) and our department. UHV model studies (TUW) addressed the specific properties of oxide supports and metal nanoparticles via surface science methods, focusing on the nature of interaction and reaction with reactants and products. Novel, robust and stable nanostructured catalysts were expected to facilitate a successful transition from noble to base metals: ZrO_2 supported Ni and Pt catalysts were synthesized in our laboratory and distributed among the co-operating partners. TUM carried out kinetic and sophisticated structural measurements on these and their own catalysts. However, only the results obtained in our laboratory will be discussed in the present report.

1.2. Objectives of our research

The objectives of our research were 1) to develop highly active and stable catalysts possibly without any noble metal, 2) test them under realistic conditions using a model biogas composition, 3) investigate the elementary reactions with labeled reactants 4) determine the coke structure and its formation routes on each catalyst system and finally, 5) based on the results give feedback to catalyst synthesis.

As for task 1), the preparation methods were chosen based on our experience and the relevant literature on how to hinder coke formation (adding a promoter, decreasing particle size, combination with noble metal, etc). Pt, Ni and bimetallic PtNi/ZrO_2 catalysts were prepared in different ways with and without sodium promotion, as among alkali metals, the effect of sodium on the properties of ZrO_2 supported Ni or Pt catalysts was rarely investigated. Sodium was introduced prior to or simultaneously with the metal precursor. We have a great experience in using noble metal sols for the preparation of heterogeneous catalyst (when metal ions are reduced to nanoparticles in liquid phase then adsorbed onto a solid support). Here we expected the decrease of particle size via the fast aqueous reduction of metal precursors with $NaBH_4$, and in the case of bimetallic samples, a better intermixing of Pt and Ni.

To fulfill tasks 2-4), several technical developments were planned and realized during the time frame of the project. A lot of time and energy were required to set up those systems and run routinely, and so they deserve to be discussed a bit longer in the experimental part.

2. Experimental part

2.1. Sample synthesis

Table 1 summarizes the main points of sample preparation. The dried solid samples were calcined in air at 600 °C and reduced in H_2 at 600 °C for 2 hours and stored in air before further use (these are referred to as received samples from now on). The main difference between the sol-method and the traditional incipient wetness or the long-lasting modified aqueous impregnation we applied is the following: in the latter cases the first reduction step is carried out on the metal oxide support, while in the former case reduction is done by $NaBH_4$ in water. Note, that the sol-derived samples during the initial pretreatment were also calcined and reduced to remove the residues of the synthesis. However, the final as received sol-derived catalysts differ from the others even if the same metal loading and support material were used. Our aim was to control and influence the metal-support interaction and catalyst structure in the same macroscopic Ni(Pt)-ZrO_2 system.

Prompt Gamma Activation Analysis (PGAA) was used to determine metal loadings for the sol-derived samples. Due to the nature of the impregnation method (no way of metal loss) metal content

can be taken as the nominal value for the rest of the samples. Na content was ascertained for Zr8Ni1_Na by PGAA.

Table 1. The prepared samples, metal loading and the corresponding synthesis routes

Sample name	Metal content	Preparation procedure
Zr6 support	-	Calcination of Zr-hydroxide (MEL Chemicals) at 600 °C
Zr8 support	-	Calcination of Zr-hydroxide (MEL Chemicals) at 800 °C
Zr6Ni3_iw	3 wt% Ni	Incipient wetness of Zr6 at RT with Ni-nitrate
Zr8Ni1_iw	1 wt% Ni	Incipient wetness of Zr8 at RT with Ni-nitrate
Zr6Ni3_Na	3 wt%, 0.6 wt% Na	Modified 4-5 h aqueous impregnation[35] with Ni-nitrate and $NaHCO_3$ at 70 °C at a starting pH of 6.5
Zr8Ni1_Na	1 wt%, 0.6 wt% Na	The same as in case of Zr6Ni3_Na
Zr6Na support	0.6 wt% Na	Modification of the base ZrO_2 support with $NaHCO_3$ the same way as the Na-modified catalysts were prepared and pretreated
Zr6NaNi3_iw	3 wt% Ni, 0.6 wt%Na	incipient wetness impregnation of Zr6Na support with Ni-nitrate at RT
Zr8Ni1_sol	1.23 wt% Ni	Sol based method: $NaBH_4$ reduction of Ni-nitrate at 60 °C PVA and sodium-citrate stabilizers, then a post-reduction in the presence of support (suspension) and PDDA polycation. Fast handling during washing (dissolution!).
Zr6Ni2Pt1_sol	2 wt% Ni, 1 wt% Pt	The same as the monometallic sol sample but with H_2PtCl_6 and Ni-nitrate solutions
Zr6Ni2Pt1_iw		Incipient wetness at RT with both metal precursor solutions
Zr6Ni2Pt1_Na		The same as Zr6Ni3_Na but with both metal precursor solutions
Zr8Pt1_iw	1 wt% Pt	Incipient wetness at RT with Pt precursor solution
Zr8Pt1_Na	1 wt% Pt, 0.6 wt% Na	The same as Zr6Ni3_Na but with Pt precursor solution

2.2. Catalyst characterizations: ordinary technics and newly developed methods

In our Micromeritics AutoChem 2920 catalyst characterization system the reduction properties of the oxidized catalyst samples (temperature programmed reduction, TPR) were investigated usually after calcination at 700°C. CO pulse chemisorption measurements were conducted in the same instrument. After the CO pulses, temperature programmed desorption (CO-TPD) experiments under He flow were carried out up to 700 °C and monitored with mass spectrometer (QMS). The phase composition of crystalline components was investigated by X-ray powder diffraction (XRPD) analyses. A full profile fit method with corrections for preferred orientation and microabsorption let us estimate the Ni particle size even if the diffraction peaks of metal and oxide are overlapped. The morphology and structure of the catalysts and the carbon contamination after dry reforming tests were studied by (high resolution) transmission electron microscopy. For the determination of

surface elemental composition, X-ray photoelectron spectroscopy (XPS) measurements were applied. The samples were measured after in situ calcination/reduction at 600˚C, because the atmospheric pretreatment chamber connected to the UHV chamber with a load lock gate allows us to do pretreatments without contacting the sample with air.

Diffuse Reflectance Infrared Fourier Transform Spectroscopy (DRIFTS) was applied to study the catalyst samples under different conditions and gas atmospheres (CO chemisorption or dry reforming, etc). The introduced gas flow directly passed over the upper surface of the catalyst placed in the heatable sample holder (up to 500 ºC) of the Specac DRIFT environmental chamber facing the zinc-selenide window. As will be seen below, part of our catalytic investigations focusing on the mechanism of dry reforming and the carbon deposition routes were carried out at sub-atmospheric system. A great desire was to know what kind of adsorbed species are present under those conditions and what their bond strength is, when evacuation of sample is done. This is why a complete vacuum system able to pump down to 10^{-3} mbar (the same value as in the circulation catalytic system) was designed and built to our DRIFTS environmental cell. This set-up allows one to carry out measurements during atmospheric flow or in vacuum at the pressure of our interest. The system is shown in Fig. 1.

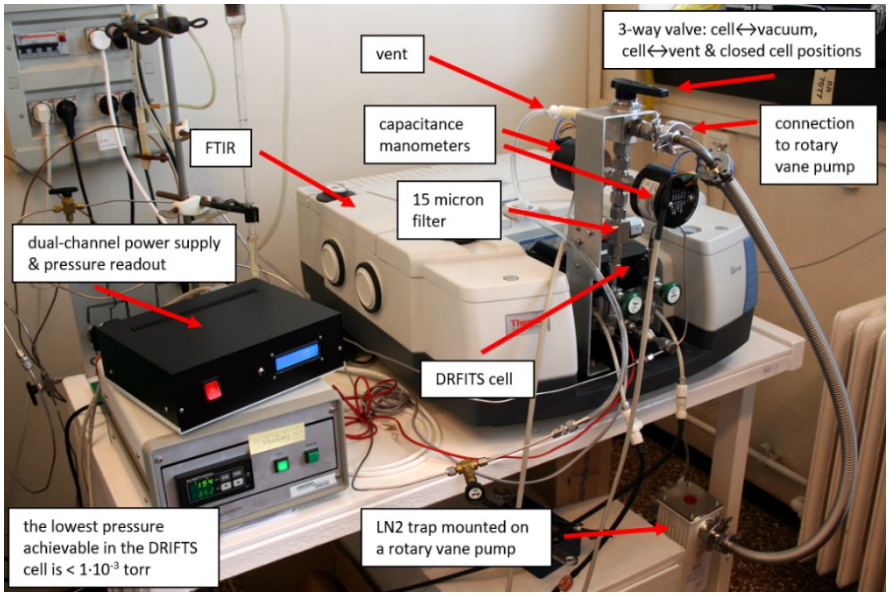

Fig. 1. Nicolet iS50 FT-IR instrument equipped with a vacuum system to carry out static DRIFTS measurements under sub-atmospheric pressure in presence of dry reforming or any type of gas mixtures.

2.3. Catalytic measurements: activity and stability tests under traditional conditions or mechanistic studies in newly constructed systems

2.3.1. Catalytic and TPO measurements in a traditional fixed bed reactor at 1 atm flow.

Two types of catalytic tests (short and stability tests) were done in the fixed bed reactor at 1 atm using CH_4:CO_2:Ar = 68:31:1 mixture (from now on this is referred as DRM mixture for the sake of simplicity). Extremely high concentration of methane was set to mimic biogas composition which is not common in the literature. Short dry reforming tests after in situ reduction at 600 ºC were started with a temperature ramp to 600°C followed by a 2 h hold time. For the long term 24-hour isothermal stability test the sample was reduced at 750 ºC with and reaction was initiated at 675ºC after He purge of H_2. A quadrupole Pfeiffer Prisma mass spectrometer was connected via a differentially pumped quartz capillary to the reactor outlet. Due to the reaction stoichiometry - that causes volume flow increase at the outlet of the reactor - argon was used as an internal reference gas for calculation of the outlet mass flows, to determine H_2/CO ratio and methane and carbon dioxide conversion values after adequate calibration. The following mass signals as representatives of the gas components were measured: 2-H_2, 15-CH_4, 28-CO, 44-CO_2.

Temperature programmed oxidation (TPO) measurements were conducted in the same flow system to detect and measure carbon deposits formed in the DRM reaction after calibration.

2.3.2. Catalytic and TPO measurements at sub-atmospheric pressure in a newly developed closed loop circulation system using $^{13}CO_2$.

An all-glass circulation system shown in Fig. 2 was built and applied to conduct isotope-labeled reactions at sub-atmospheric pressure. In this setup 25±0.5 mbar CH_4 (containing 2% Ar) and 25±0.5 mbar $^{13}CO_2$ (99 % purity, producer: Consigour Ltd.) was applied. The system could be separated into the gas blending space and the reactor space, and these two could be merged when needed. Reactants were introduced by measuring the sequential pressure with a capacitance pressure gauge in the gas blending space. Circulation was carried out by a double-acting piston pump. During the experiments, the overall system (p=50 mbar for DRM and p=200 mbar for TPO) was monitored through a fine glass capillary connected to a Pfeiffer Prisma quadrupole mass spectrometer. DRM experiments in this circulation system are able to provide only qualitative results due to the nature of the capillary inlet system and the significant pressure increase during the reaction (MS calibration of all components would be elusive). The following mass signals were taken as the representatives of the gas components: 2-H_2, 15-CH_4, 17-$^{13}CH_4$, 28-CO, 29-^{13}CO, 40-Ar, 44-CO_2, 45-$^{13}CO_2$. The sample in the U-shaped quartz reactor tube could be reduced in H_2 flow (there is an outer connection point for such purpose) at 600 °C then cooled to 150 °C and evacuated to about $1.5*10^{-2}$ mbar pressure. There were 2 types of catalytic experiments ending with TPO measurements. In one case, the premixed reactants were introduced onto the reduced, evacuated sample at about 150 °C, afterwards temperature was ramped up to 600 °C with 10°C/min rate and held there for 30 min, then evacuated and cooled close to room temperature before the TPO measurements (ramp-hold type experiment). The other type of measurements were the isothermal runs at 600°C, which means that the reduced sample in the reactor space was heated in vacuum to 600 °C, then the reactant mixture was introduced onto the catalyst, and after 30 min it was evacuated, then cooled down for the start of TPO. The terminal TPO measurements were carried out by adding 200 mbar oxygen to the evacuated catalyst and ramping the temperature again to 600 °C. The CO_2 signal (CO alone was not formed) detected at m/e=44 and m/e=45 was differentiated to get a peak-shaped curve instead of the original integral signal. The CO_2 signal could be calibrated and the surface coke evolving as gas phase labeled or unlabeled carbon dioxide was quantified.

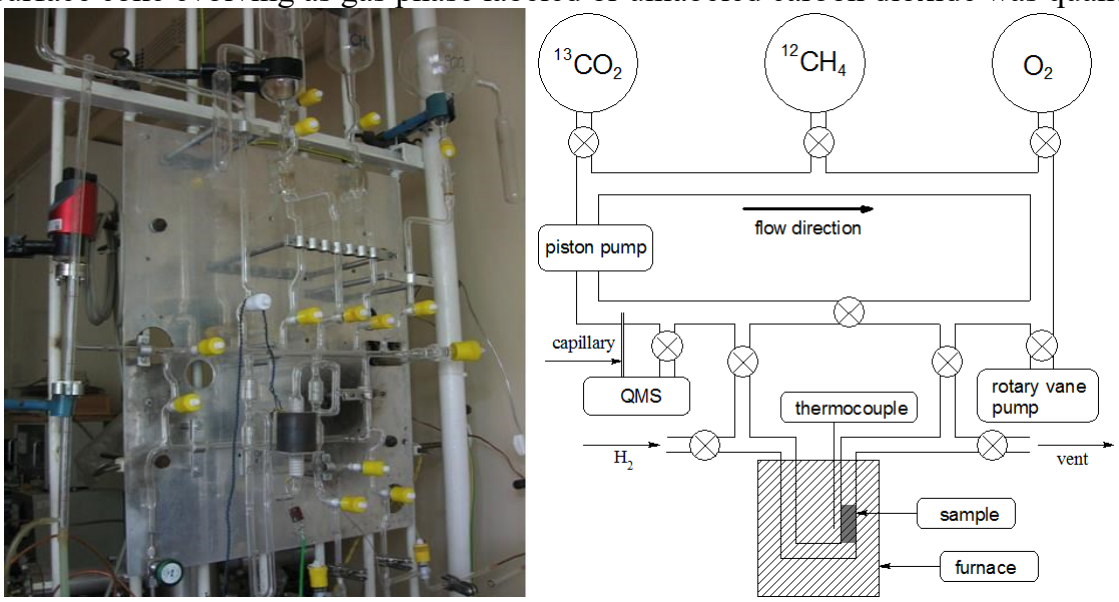

Fig. 2. Closed loop circulation system used in the $^{13}CO_2$-labeled dry reforming experiments for mechanistic studies

2.3.3. Steady State Isotopic Transient Kinetic Analysis (SSITKA) using a custom-made Micromeritics AutoChem flow system connected to a Pfeiffer QMS

Steady State Isotopic Transient Kinetic Analysis (SSITKA) was developed by Goodwin et al.[36] as a technique for studying complex surface reaction mechanisms under realistic - in comparison with UHV techniques - operating conditions of the catalyst. In distinction to other transient response techniques, in SSITKA we generate a very fast isotopic step function and record the transient response of the system with a mass spectrometer. In our case nothing, only the carbon atoms of the CO_2 reactant are changed abruptly for ^{13}C. In the absence of kinetic isotope effects, these transients let the overall surface occupancy unperturbed and therefore give access to the mean surface-residence time and the abundance, surface coverage of adsorbed intermediates leading to the product. As it was mentioned in the introduction, only SSITKA is able to measure the – usually very low – surface coverage of active carbon that truly participates in the formation of CO. As the theory behind this kind of measurements is quite complex and no one in Hungary deals with SSITKA, we needed more time to set up, purchase gases, ascertain the conditions, and do the first preliminary SSITKA measurements on two Ni/ZrO_2 samples. The instrument schematic is shown in Fig. 3.

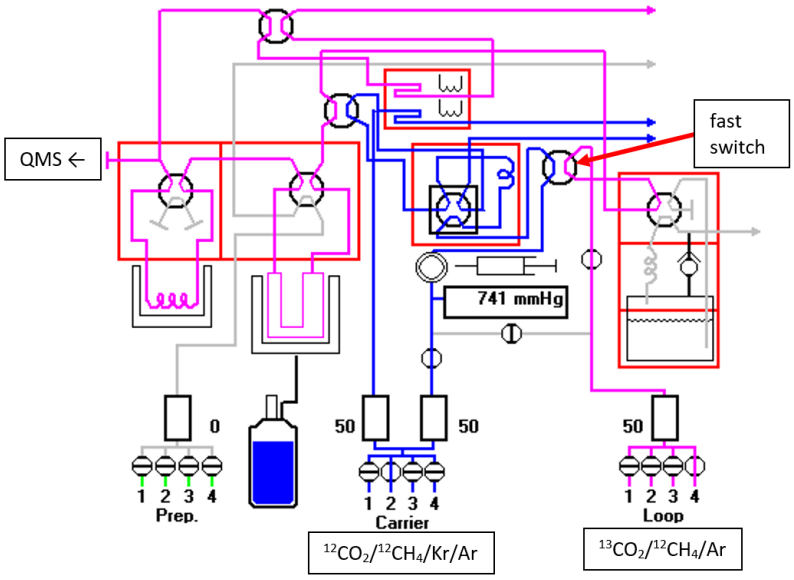

Fig. 3. Scheme of our MIC AutoChem 2920 system with fast switch function for SSITKA experiments

3. Results: dry reforming studies on Ni/ZrO_2 catalysts

3.1. Catalyst characterization: dispersion, TPR, XPS measurements and CO chemisorption

To enhance basicity of the catalysts and so CO_2 adsorption capacity, Na_2O promotion was done in 2 different ways and compared to the bare Ni samples prepared by incipient wetness. The relatively long, mild heat treatment during preparation of Zr6Ni3_Na was done deliberately hoping to get some Na^+ inclusion into the Ni phase to achieve localized promotion of Ni with a minute amount of Na and the high dispersion of sodium on the ZrO_2 surface. We suppose that during preparation, basic Ni carbonate formed by polymerization of aqua-hydoxo complexes of Ni^{2+} according to ref.[37] As for the Zr6NaNi3_iw sample, Ni loading was done on the Na-modified, calcined, reduced support. This produced significant differences between the samples. Metal loading was varied to get higher dispersion, if possible, in the case of 1 $\%Ni/ZrO_2$ samples. As for

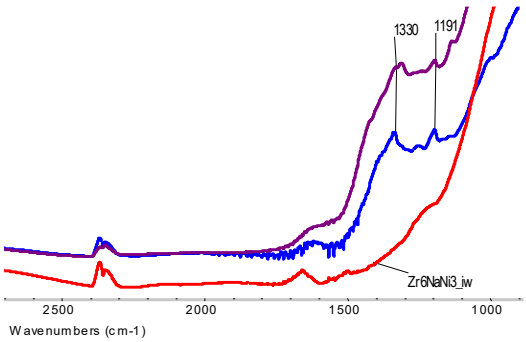

Fig. 4. DRIFTS spectra of sol-derived Pt and NiPt samples showing boron-oxide peaks on the surface compared to a reference B-free sample (Zr6NaNi3_iw).

the sol-derived catalyst, PGAA measured a minute, 0.09 wt% B content, probably remained from the reducing agent, which gave FTIR peaks at 1330 and 1187 cm^{-1} assignable to the asymmetric B–O bond stretching vibrations of a dispersed B_xO_y phase[38,39] that was not seen on the rest of the samples (see Fig. 4). This B contamination might also play a role in the coking behavior of the catalyst, because according to the literature, deliberate boron promotion may have positive effect in dry reforming in a certain concentration range on Al_2O_3 supports (at much higher concentrations than we have here).[40,41] Determination of Ni size in the ZrO_2 supported samples turned to be difficult by TEM due to the lack of sufficient contrast between the crystalline oxide support and the Ni particles. Metal particle size estimated by XRD could not provide firm results either, because the Ni (111) and the monoclinic baddeleyite ZrO_2 peaks overlapped. We could estimate Ni particle size only for the 3 % Ni-loaded catalysts to be around 20 nm, the low-loaded samples had no sign of Ni in the XRD curves. CO pulse chemisorption (see Table 2) was also done to measure Ni dispersion: low Ni dispersion values were obtained for all samples, which is not a surprise after 700 °C oxidation and reduction treatments for Ni (easily sintering metal). We must emphasize that these data were calculated by assuming CO:Ni=1 chemisorption stoichiometry, but they are underestimated, because real CO bonding was not linear according to the DRIFTS results (see later). The other reason of the extremely low dispersion of Na-modified catalysts that sodium(oxide) depresses the CO chemisorption, if Ni surface is partially covered after the high temperature reduction as it was reported for Li, Na or K-doped Ni catalysts.[34,42,43] Similar conclusion was drawn in the case of Ni-CaO-ZrO_2 catalysts prepared by co-precipitation, when decoration of Ni by the support itself was thought to be the reason of the low dispersion measured by H_2 chemisorption.[44] Balakos et al.[30] also pointed out that changes during surface composition with reduction and reaction conditions gives rise to uncertainty in H_2 chemisorption based activity data. According to our results and the adequate literature, we might assume that a part of Ni surface is electronically influenced or physically covered by Na_2O or Na_2CO_3 patches during CO chemisorption on the Na_2O-promoted catalysts.

Next, the temperature programmed reduction measurements will be discussed. TPR results of the oxidized samples are summarized in Fig. 5 and Table 2. Note, that 3% Ni (II) (NiO) would give 11.46 cm^3/g_{cat} H_2 consumption, while 1% NiO content would give 3.8 $cm^3/g_{cat,}$ while 1%Ni(III) (Ni_2O_3) would result 5.73 cm^3/g_{cat} H_2 consumption. Considering this, we can conclude about 100 % reducibility for the 3% Ni/ZrO_2 samples and the higher H_2 consumption for low-loaded samples assumes the presence of higher oxidation state Ni species, especially in the case of Zr8Ni1_sol and Zr8Ni1_imp. The NiO in weak interaction with the support was present in a considerable amount on the iw samples and reduced at around 315 °C. The NiO_x species in stronger interaction with the support[44] were reducible at 410-430 °C on these samples but only at 490 °C in the case of the sodium-containing counterparts. It seems that the Na-incorporation resulted in a NiO_x phase that is relatively hard to reduce. The sol-derived catalyst is a transition between the two other types reflecting different Ni-oxide structure and reduction behavior.

Table 2 also summarizes the Ni and Na surface concentrations obtained by XPS investigation after in situ calcination/reduction treatment at 600 °C. Considering the bulk sodium content, Na/Zr_{bulk} would be 0.03, but it is straightforward that Na is segregated and well dispersed on the surface, because Na/Zr_{surf}=0.83 or 0.94 for Zr6Ni3_Na and Zr8Ni1_Na, respectively (in the reduced state). Note that the ZrO_2 support itself contain insignificant amount of Na impurity as data on the iw sample reflects.

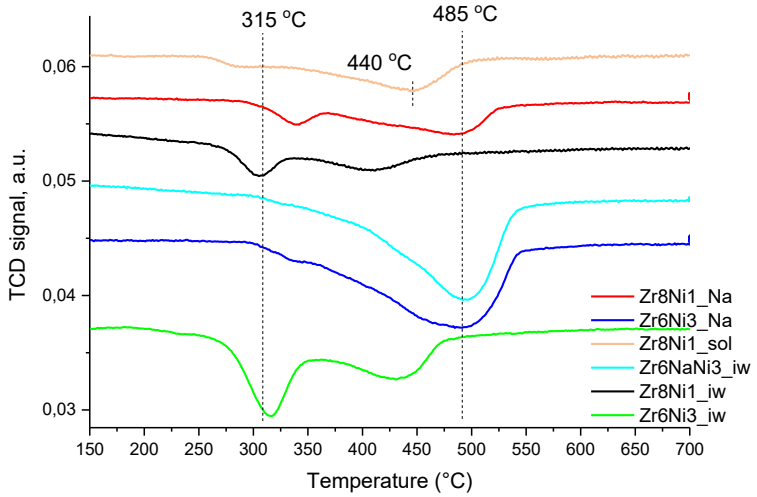

Fig. 5. Results of temperature programmed reduction on preoxidized Ni samples

A simple rough estimation supposing monolayer coverage of ZrO_2 with Na_2O reveals that maximum 20% of ZrO_2 surface might be covered on Zr6 and 32 % on Zr8 (37 m^2/g BET surface area of Zr6 and 22 m^2/g for Zr8 was used in the calculation). Thus, it should be accepted that sodium exists either as small Na_2O islands on the support or integrated into the ZrO_2 network forming diluted structures of Na_2ZrO_3. This possibility is really important since bulk Na_2ZrO_3 was found a highly efficient high temperature (T>500 °C) CO_2 absorbent that can bind and at release CO_2 depending on the temperature and partial pressure of the gas ($CO_2+Na_2ZrO_3 \rightleftharpoons Na_2CO_3+ZrO_2$) according to refs.[45, 46] The measurement of Na/Zr_{surf} for the Na-premodified catalyst (Zr6NaNi3_iw) is under progress now, but based on the other results (see later), we suppose that the same amount Na has a distinctly different distribution on Zr6NaNi3_iw.

Table 2 Dispersion and the XPS surface concentrations in reduced state of the Ni samples

sample name	Ni dispersion by CO pulse chemisorption[a]	H_2 consumption during TPR cm^3/g_{cat}	XPS surface concentration[b]	
			Ni/Zr	Na/Zr
Zr6Ni3_Na	0.9 %	12.0	0.07	0.83
Zr6Ni3_iw	2.2 %	12.1	0.04	0.08
Zr6NaNi3_iw	1.8 %	12.9	-	-
Zr8Ni1_iw	3.6 %	4.7	-	-
Zr8Ni1_sol	3.0 %	5.6	0.13	0.25
Zr8Ni1_imp	1.3%	5.4	0.03	0.94

a: After TPR measurements assuming CO:Ni=1 stoichiometry
b: After in situ calc/red treatment at 600 °C

XPS investigation of the C 1s region discovered at 288.8 eV a carbonate type carbon in the calcined state of Na-modified samples. It means that some carbonates are strongly held by the sodium dispersed on the ZrO_2 support. After in situ reduction they disappeared and a little adventitious carbon remained only on the surface.

The Na 1s peak after calcination and reduction was detected at 1071.9 eV. This Na_2O must be spread over the ZrO_2 and connected to ZrO_2 via Na-O-Zr entities. There was a small shoulder at an unusual low binding energy at around 1068 eV on Zr6Ni3_Na. This type of sodium supposedly belongs to a species in intimate contact with nickel.

Fig. 6 a) depicts that the Ni in the calcined state of Zr6Ni3_iw corresponded to Ni^{2+} in NiO phase. Over the sodium-promoted calcined catalysts nickel signal could be fitted with NiO and at higher BE values with Ni-hydroxide (Ni^{2+}) on Zr6Ni3_Na (855.9 eV), while Ni^{3+} was also present probably as NiOOH on Zr8Ni1_Na (856.8 eV, not shown here). This $Ni(OH)_2$-NiOOH is

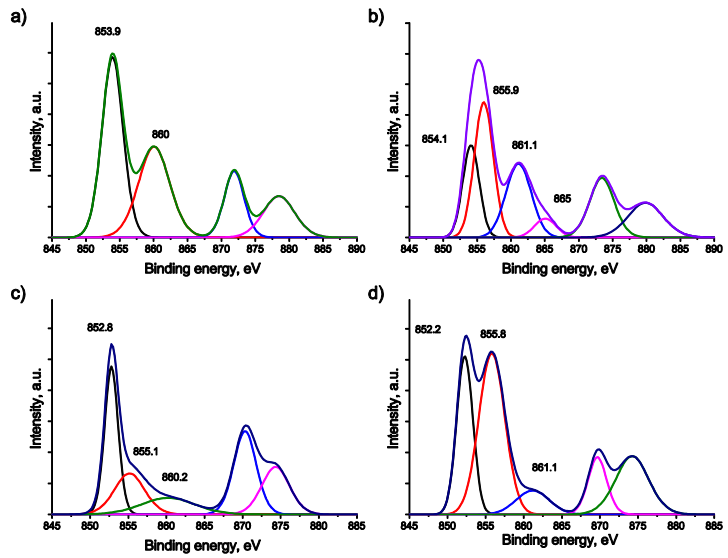

Fig. 6. Ni 2p region measured by XPS after calcination at 600 °C on a) Zr6Ni3_iw and b) Zr6Ni3_Na; and after reduction at 600 °C on c) Zr6Ni3_iw and d) Zr6Ni3_Na. Fitted curves are shown.

supposedly responsible for the stronger oxide-support interaction as was observed during TPR measurements and also for the higher H_2 consumption of Zr8Ni1_Na. As for the Ni oxidation state in reduced form of the samples there is metallic Ni on Zr6Ni3_iw (Fig. 6. c) and Zr8Ni1_sol (not shown here), but on the sodium-promoted samples – besides metallic Ni – there is still a significant contribution at 855.8 eV corresponding to Ni^{2+} most probably in a NiO_xH_y species, the more was measured on Zr8Ni1_Na. This surface hydroxide-like nickel compound seems to be very stable even under reducing atmosphere, although TPR suggested almost complete reduction of Ni-oxide at 600 °C. This might be explained if we assume a well dispersed, thin layered form of Ni hydroxide. The extremely low intensity satellite peak (Fig. 6 d) compared to what one would expect based on the intensity of the apparent $Ni(OH)_2$ (~NiO_xH_y) component suggests that some unique electronic interaction prevails between nickel and other element(s), or even could be the sign of a mixed phase or alloy formation. We suppose that sodium ion is embedded in the NiO_xH_y-Ni matrix resulting in a decreased satellite intensity. It was reported[47] that the interaction of potassium with an oxidized Ni(110) single crystal during annealing resulted Ni^{3+} species probably as potassium nickelate (K_2O_2+2NiO=2$KNiO_2$). We even may assume the same in our case, viz. the formation of sodium nickelate ($NaNiO_2$) especially for Zr8Ni1_Na. We suggest that under reducing atmosphere similar to the classic strong metal support interaction (SMSI) develops in the promoted catalyst and part of the metallic Ni surface is surrounded/buried by a Na-O-Zr network.

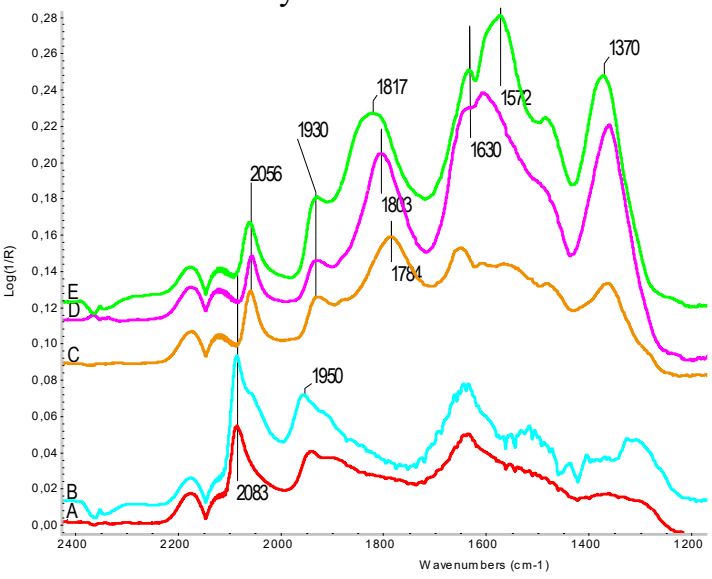

Fig. 7. DRIFTS spectra in 1%CO/He at 25 °C on A) Zr8Ni1_iw, B) Zr6Ni3_iw, C) Zr6NaNi3_iw, D) Zr8Ni1_Na, E) Zr6Ni3_Na

CO chemisorption was measured with DRIFTS method to compare the different Ni sites (Fig. 7). Linear CO on Ni metal[48] was seen at lower wavelength in the case of Na_2O-modified catalysts and the band at around 1800 cm^{-1} due to the alkali promotion.[49,50] (The band at 1638 cm^{-1} is assigned to the bending mode of H_2O). We certainly assign the peak at around 1820 cm^{-1} to CO adsorbed on Ni sites that are influenced by sodium or located in close vicinity of sodium, viz. at the metal-support interface. We even may suppose the existence of a tilted CO molecule with the oxygen end bond to Na^+.[51] Since that sodium promotion can change the typical IR frequency of a chemisorbed molecule via strengthening or weakening of a given bond, the peak assignment in the carbonate region is very difficult and the formate bands are virtually indistinguishable from those of

carbonates.[52] Keeping this in mind, the bands at 1572 cm^{-1}, 1475 cm^{-1} and 1370 cm^{-1} are assigned to the presence of carbonate species[53] on the sodium-promoted samples.

3.2. Catalyst activity in fixed bed flow reactor and investigation of the spent samples by TEM and TPO

Experiments in the tubular reactor were carried out with CH_4:CO_2:Ar = 68:31:1 mixture at atmospheric pressure in two manners: i) short tests with temperature ramp and hold (2h) and ii) stability tests after a 700 °C reduction treatment at constant 675 °C reaction temperature. The catalytic performance of chosen samples were studied only in the short tests and they were not significantly different: all samples were active and the sodium-promoted ones reached higher CO_2 conversion than the rest of the samples. Coke did not form on Zr8Ni1_Na. A representative TEM/HRTEM image of the spent Zr6Ni3_Na is shown in Fig. 8.

The carbonaceous deposit on Zr6Ni3_Na was composed of partly by disordered carbon nanotubes. We observed an amorphous layer or shell on the support particles (signed with arrows) that could be also carbonaceous deposits. HRTEM shows a close look of a 22 nm Ni particle at the end of a carbon nanotube: the lattice period 2.00-2.01 Å measured at the outer line or the border of Ni particle may represent (113) Ni_3C, the 2.05 Å might be a strained Ni (111) and the one with 2.08 Å spacing is assigned to NiO (200) lattice. The largest measured period of 2.36 Å fits neither Ni, nor Ni-carbide, however, it can be indexed as (011) of $Ni(OH)_2$ or (011) of NiOOH spacings.

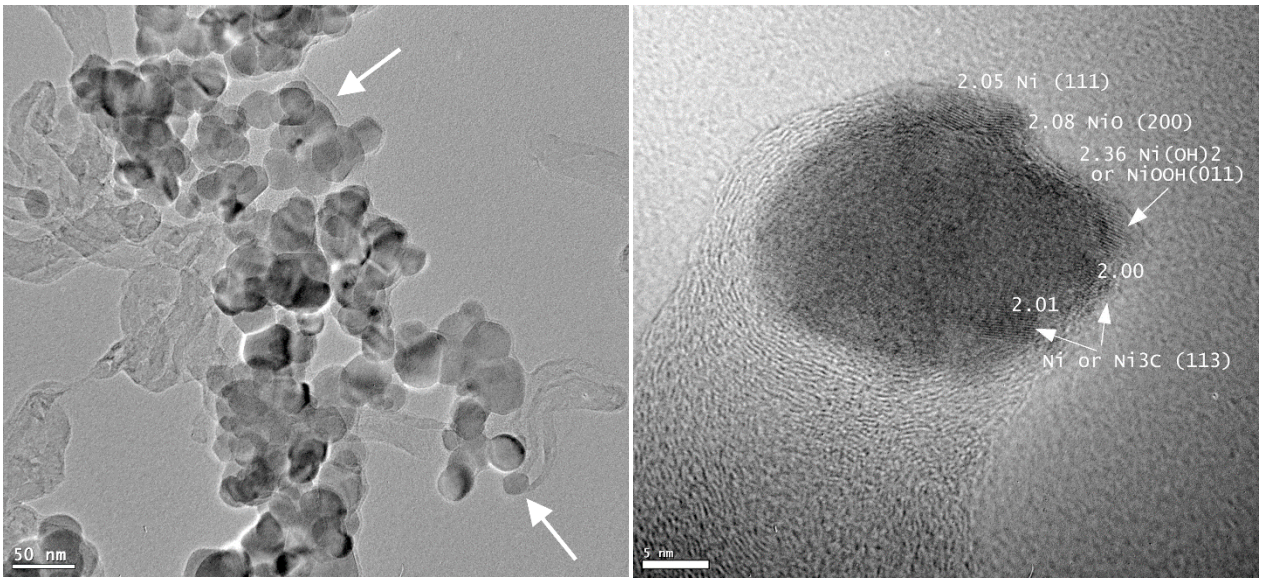

Fig. 8. TEM images taken after DRM at 600 °C (short term catalytic test) on Zr6Ni3_Na. Left: structure of amorphous carbon and nanotube with Ni particle at the tip. Right: HRTEM image of a single Ni particle at the end of a nanotube

We can thus declare that NiO, probably $Ni(OH)_2$ and Ni/Ni_3C exist beside each other in small patches or domains of the metal surface. (Indeed, we cannot prove if the oxidized forms of nickel were formed during the reaction or after the handling of the spent sample in air.) We tentatively suggest that the neighboring Ni species with different oxidation state keep the particle active, since these kinds of nanodomains – making a "ruffled" Ni look – were also seen on other metal particles of this sample, while none was observed on Zr6Ni3_iw.

The results of the long term – 24 h – catalytic runs are depicted in Fig. 9. In this case significant differences were seen: Zr6Ni3_Na was the most active and quite stable, Zr6Ni1_Na and Zr8Ni1_sol slightly deactivated, then Zr6NaNi3_iw was in between the former ones and the completely deactivated iw samples. On Zr6Ni3_Na the deactivation rate in terms of CH_4 and CO_2 seemed to be very similar. This suggest that the CH_4 and CO_2 activation routes are equally working and well balanced. TEM showed that numerous long nanotubes were formed on the iw samples and some of

them contained encapsulated Ni particles at the tips, while much less carbon nanotube was found on Zr6Ni3_Na.

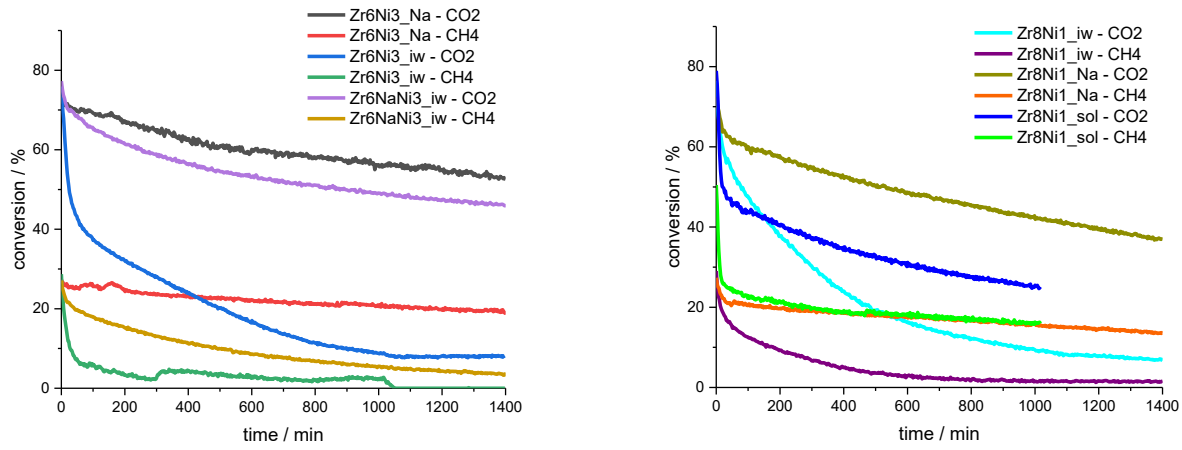

Fig. 9. Methane and CO_2 conversion curves during long term stability run at 675 °C on left side) 3 wt%Ni samples and right side) 1 wt% Ni samples. DRM conditions: after reduction at 750 °C/0.5h cooling to T=675 °C in He, then DRM with CH_4:CO_2:Ar = 68:31:1 mixture

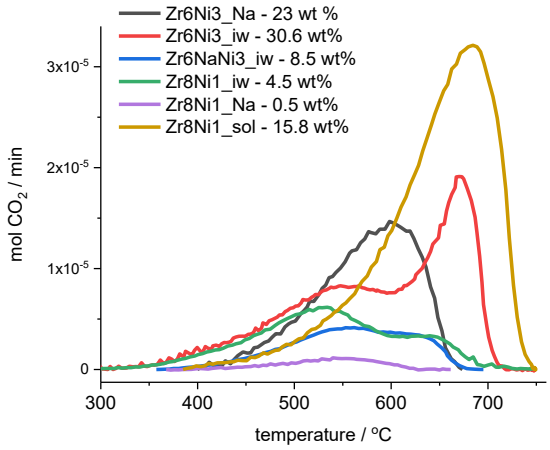

The deposited coke was oxidized by TPO measurements (Fig. 10). Both unpromoted sample had a first TPO peak at around 520-530 °C and a second more definite one at 640-670 °C, but on the low loaded sample less carbon was formed. The complete deactivation should be explained by the buried Ni particles and not by strong sintering, because d>50 nm particles (either ZrO_2 or Ni) were not observed by TEM. It is interesting that Zr8Ni1_Na was as active as Zr8Ni1_sol while it produced negligible amount of inactive coke with a much higher CO_2 conversion suggesting its role in carbon removal during the DRM process.

Fig. 10. TPO curves and the carbon content in wt% after the stability tests

The 15.8 wt% carbon was oxidized at the highest temperature on the sol-derived catalyst in a long pre-tailed single peak, still, the sample was active after 24 hours under our severe conditions. Analyzing all these data, we suggest that catalyst has high deactivating tendency if the ratio of carbon removable at around 520 °C to the total carbon is significant. The coke on all the promoted catalyst is a very mobile and reactive type and it can be removed completely at the lowest temperature. However, the way of sodium addition matters: the pre-modified catalyst (Zr6NaNi3_iw) cannot maintain its activity, probably because the active sites are covered by inactive coke, while on the Na_2O-promoted samples the surface carbon is transferred continuously away from the active sites. The sol-derived catalyst is an interesting combination – if the B_xO_y residue located close to the Ni-ZrO_2 interface – can provide active OH species to remove coke from the working sites according to the literature.[40,41]

3.3. Mechanistic studies

3.3.1. CO-TPD and DRIFTS studies

The different surface properties of the catalysts are also reflected in CO-TPD experiments in He flow carried out after CO pulse chemisorption (Fig. 11). The desorbing species were H_2, CO, CO_2 and H_2O from all catalysts. Note that H_2 and H_2O simultaneously desorbed below 200 °C only from the sodium-promoted catalysts and the sol-derived one.

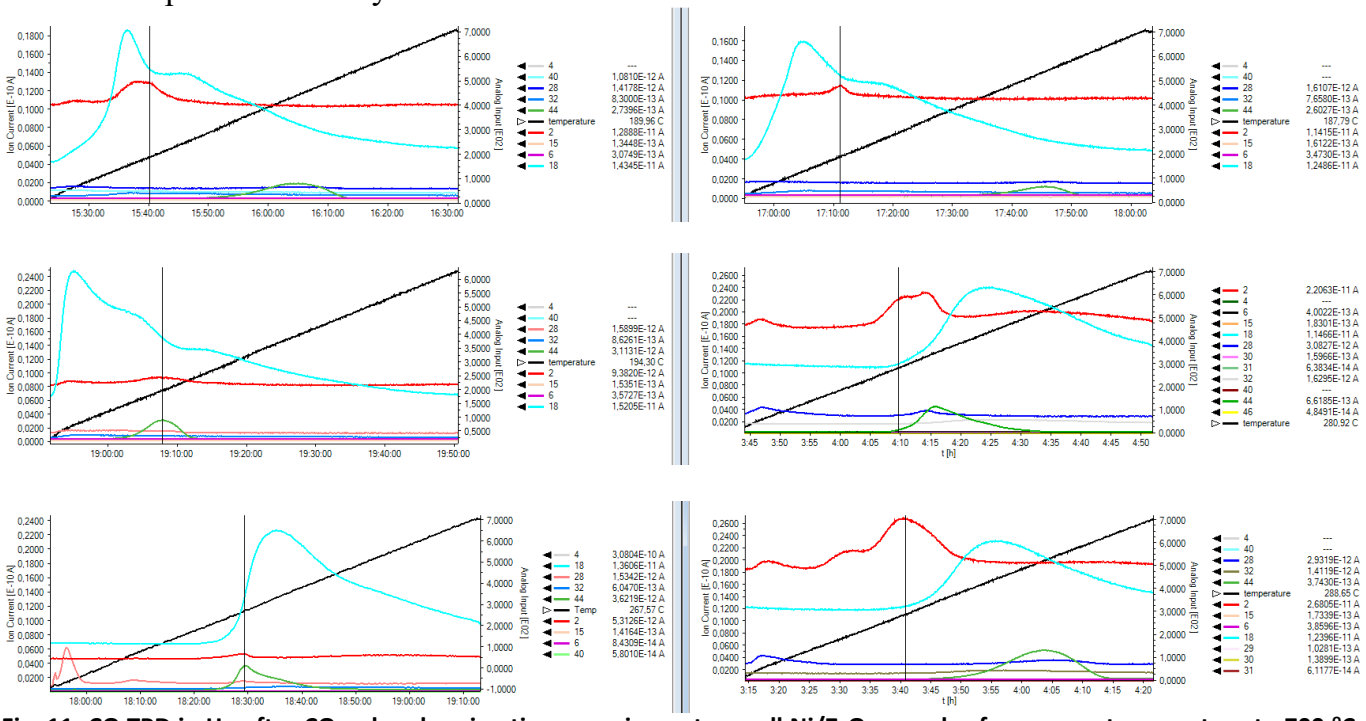

Fig. 11. CO TPD in He after CO pulse chemisortion experiements on all Ni/ZrO_2 samples from room temperature to 700 °C. First column from top to down: Zr6Ni3_Na, Zr8Ni1_sol, Zr6Ni3_iw. Second column from top to down: Zr8Ni1_Na, Zr8Ni1_iw, Zr6NaNi3_iw. (H_2: red, H_2O: light blue, CO_2: green, CO: dark blue). The temperature is depicted on the right y axis and its actual value at the vertical line is shown in each legend as "Temp" in °C.

Considering the presence of chemisorbed CO on Ni/NiO_xH_y and the hydroxyls of the support, a surface water-gas shift reaction ($CO+H_2O \rightleftharpoons H_2+CO_2$) may proceed producing H_2 and CO_2 through a formate (or other) intermediate. The latter is decomposed to H_2 and CO_2 at low temperature[54] but the CO_2 re-adsorbs and desorbs together with the stable carbonates of the support at higher temperature. Note the characteristic H_2O profile of the three catalysts that were considered active in the stability tests (Zr6Ni3_Na, Zr8Ni1_Na, Zr8Ni1_sol). This low temperature dehydration feature may be in connection with catalytic activity and gasification of surface coke. Based on the temperature of CO_2 signal, the basicity of the samples is the following: Zr8Ni1_sol>Zr6Ni3_iw>Zr8Ni1_iw>Zr6Ni3_Na>Zr8Ni1_Na>Zr6NaNi3_iw. This shows the higher basicity of the sodium promoted samples and the acidity assignable to B_xO_y contamination of the sol sample, as expected.

As carbonate species are considered to play a role in surface carbon removal at low temperature and at the interface of nickel and the support,[55], our aim was now to follow the conversion of IR visible surface species during temperature increase up to 500°C in the presence of the DRM reaction mixture containing 70% CH_4+30%CO_2. In Fig. 12 DRIFTS spectra on Zr6Ni3_Na and Zr6Ni3_iw in presence of DRM gas flow are compared at the lowest 300 °C and the highest 500 °C. We can conclude that bidentate formate species (2878, 1570, 1365 cm^{-1}) dominate over bicarbonates[56]

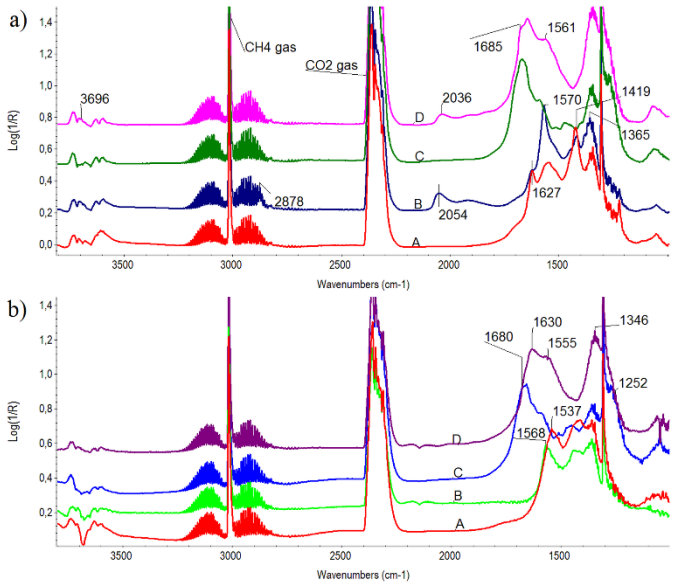

Fig. 12. DRIFTS spectra obtained in the presence of CH_4:CO_2=70:30 DRM flow at a) 300 °C and b) 500 °C. Curve A: Zr6 support, B: Zr6Ni3_iw, C: Zr6Na support, D: Zr6Ni3_Na

detected at 1627, 1419 and 1224 cm^{-1} on Zr6Ni3_iw at 300 °C . This means that via finite dissociation of CH_4 on Ni particles H_s is produced that accelerates the bicarbonate→formate transition. Chemisorbed CO on Ni is already detected at 2054 cm^{-1}. At 500 °C formate species may be still present at 1568 cm^{-1} together with mono- and polydentate carbonates (1537 cm^{-1}). As for the sodium-promoted case, the difference under DRM mixture between the support and the catalyst is not so clearly seen. On Zr6Ni3_Na, little OH at 3696 cm^{-1}, bidentate carbonates[57] at 1645 cm^{-1}, bridged bidentate carbonate[58] at 1685 cm^{-1}, monodentate carbonate at 1561 and 1350 cm^{-1} plus CO chemisorbed on Ni (at 2036 cm^{-1}) are observed at 300 °C. At 500 °C (see Fig. 12 b), the situation is very similar, except of the missing carbonyls on Ni, and the absence of band at 1680 and 1252 cm^{-1} on Zr6Ni3_Na but still having bands at 1630, 1555 and 1346 cm^{-1} (bidentate and monodentate carbonate). Although gas phase CH_4 obscures the region, we claim that there is no sign of formates at any of the temperatures on Zr6Ni3_Na under dry reforming mixture. Moreover, bridged bidentate and bidentate carbonates are present due to the sodium on the surface, the former seems to be destabilized (converted) on the Ni-containing catalyst. Here we must note that the sol-derived catalyst was the only one that kept chemisorbed CO on Ni during the temperature ramped dry reforming reaction. This means that Ni sites were not covered by coke neither formed carbide up to 500 °C.

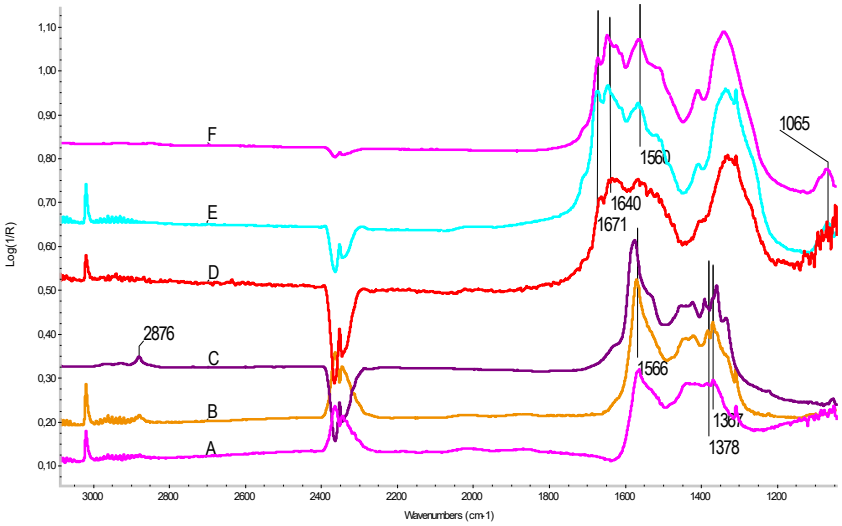

Fig. 13. DRIFTS spectra taken during the static DRM experiment at p=50 mbar followed by evacuation. In presence of DRM mixture at 500 °C on A) Zr6Ni3_iw and D) Zr6Ni3_Na; in presence of DRM mixture after cooling to 300 °C on B) Zr6Ni3_iw and E) Zr6Ni3_Na; and after the subsequent evacuation and cooling to 50 °C on C) Zr6Ni3_iw and on F) Zr6Ni3_Na

As our catalytic experiments with labeled CO_2 were carried out at sub-atmospheric pressure to study reaction steps and coke formation (see in the next sections), we have built a vacuum system attachable to the DRIFT cell to see what kind of surface species are present under reduced pressure and what is their stability against evacuation. As an example, Fig. 13 shows that the same type of carbonates/formates are detected at 50 mbar as in the atmospheric DRIFTS experiments in flow

mode, but the view is much clearer. It is seen that evacuation at 300 °C does not remove the chemisorbed surface species and definitely formate is not detected on the sodium-promoted sample. This type of experiments allowed us to detect the bicarbonate-formate transition reflected in the shift of formate bands at lower temperature (Fig. 13 curves A and C).

As an obvious step, formate formation was to be seen under the most plausible condition: during CO adsorption on the reduced samples precovered with H_2 at 300 °C. At that stage all the sodium-promoted catalysts are dehydrated compared to the Zr6Na reference (OH was seen at 3695 cm^{-1}), while there was a bridged OH at 3666 cm^{-1} on Zr6Ni3_iw, while both, terminal and bridged was observed on the bare Zr6 support (3738 cm^{-1}, 3666 cm^{-1}). Admitting 1%CO/He onto the samples at 300 °C , CO on Ni was seen on all catalysts. The formate species were detected as usually, at 1570 cm^{-1} and 1368 cm^{-1} on the iw samples and their intensity increased somewhat with time. On all the sodium-containing samples formate bands were observable at 1605 cm^{-1} and 1354 cm^{-1}. On Zr6Na and Zr6NaNi3_iw samples the intensity again increased a bit with time. These peaks are assigned to formate species bond to oxygen in the vicinity of sodium. To our surprise, (sodium)-formates at 1605 and 1360 cm^{-1} were converted on Zr8Ni1_Na to bidentate carbonates (1640 cm-1) as seen in Fig. 14. The difference between the promoted 3% Ni and 1% Ni sample is either the rate of this transformation being faster on Zr6Ni3_Na, or instead/beside of formates other intermediate forms from CO. We hypothesize that on Zr6Ni3_Na catalyst, the very low intensity of C-H bands at 2840 and 2825 cm^{-1} already at 1 min of the experiments suggests, that more carboxylates[59] (peaks at 1556 and 1506 cm^{-1}) are formed beside/instead of formates (2825, 1605 cm^{-1}) and are converted to bridged carbonates (1670 cm^{-1}), bidentate carbonates (1640 cm^{-1}) and bicarbonates (1616 cm^{-1}) that are partially hydrogenated to formaldehyde[60] (2840 cm^{-1}). As the band at 1670 cm^{-1} and 1340 cm^{-1} was not seen in during the experiment on Zr8Ni1_Na, we suggest that this kind of bridged carbonate is bond to the Ni surface and is connected to the Zr-O-Na entities as well. In the subsequent H_2 treatment (not shown here) CH_4 was detected on Zr6Ni3_Na and the 1680 and 1605 cm^{-1} bands disappeared, while methane was not detected on Zr8Ni1_Na, although the formate disappeared too. The formate bands on the iw samples and both supports were relatively stable in H_2 flow. We assume that this transition of CO towards carbonates on a reduced surface and conversion part of them in abundant H_2 gas has a big role in the gasification of surface coke during dry reforming reaction to keep the Ni sites clean. As Zr6NaNi3_iw is not so active in this respect shows that sodium distribution on its surface is distinctly different (not localized around/on Ni).

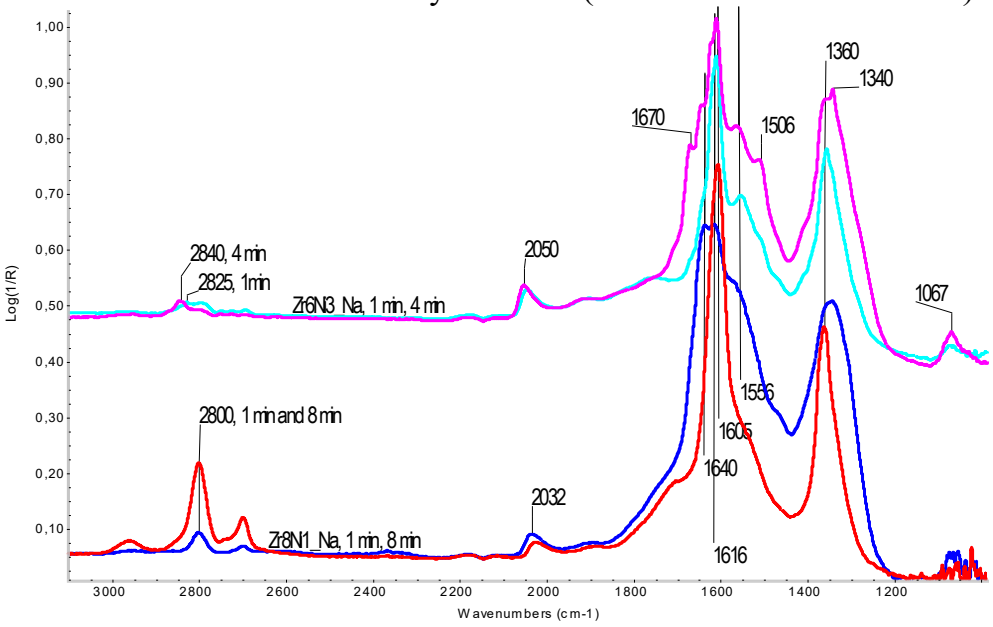

Fig. 14. DRIFTS spectra in 1%CO/He stream after H_2 treatment at 300 °C on Zr6Ni3_Na after 1 min (light blue) and 4 min (pink) and on Zr8Ni1_Na after 1 min (red) and 8 min (dark blue).

3.3.2. SSITKA studies on two chosen catalysts

Preliminary SSITKA measurements as described in the Experimental part were carried out on the best and the worst Ni catalyst in the AutoChem flow apparatus. Fig. 15 shows typical normalized transient responses following step input of the isotopic labeled $^{13}CO_2$ reactant. An inert tracer (Kr) is used to determine the gas phase holdup of the system. Note that the Kr transient response is measured in the step decay while it is calculated (according to the theory of SSITKA) in the step input to demonstrate that all other compounds have significant interaction with the catalyst. After gas phase holdup correction, the integration of the normalized step-decay/step-input response yields the overall mean surface residence time, τ of intermediate that result CO from the CO_2 activation route.

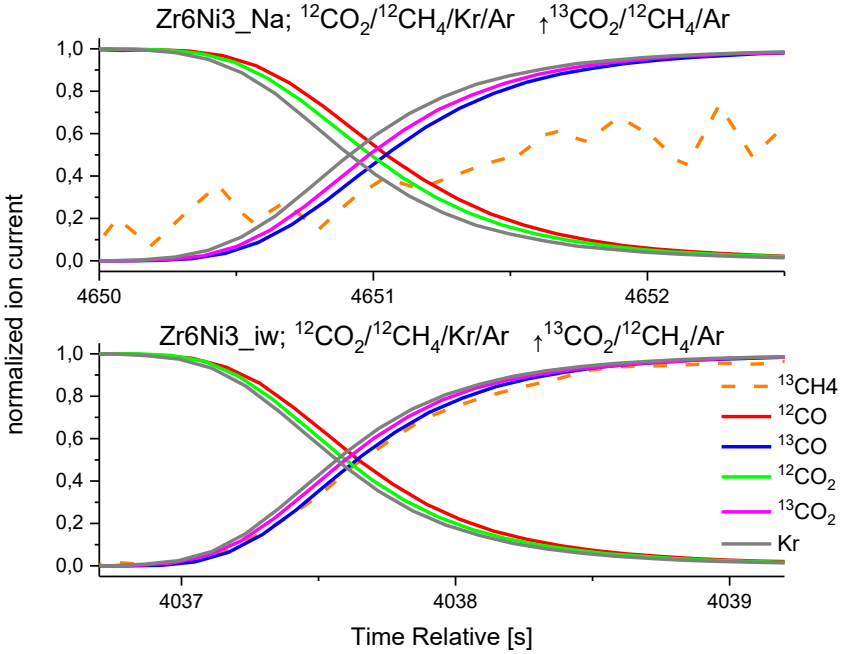

Fig. 15. SSITKA switch on chosen Ni samples with 10%CO_2:10% CH_4: 1%Kr/Ar flow at 600 °C after 1 h catalyst stabilization.

The τ on Zr6Ni3_iw was 0. 7 sec and on Zr6Ni3_Na 0.12 sec for ^{13}CO that means that the surface intermediate resulting ^{13}CO product convert much faster on the unpromoted catalyst. CH_4 conversion was 50 % for the unpromoted and 30% for the Na_2O-promoted sample. The low concentration $^{13}CH_4$ component have a noisy signal, but we still can undoubtly declare that part of $^{13}CO_2$ reactant convert to $^{13}CH_4$ on Zr6Ni3_iw while it does not on the stable and active Zr6Ni3_Na under the given conditions. This is surprising since the intermediates originating form $^{13}CO_2$ on the sodium-promoted sample stay longer before producing the ^{13}CO product but still do not hydrogenate to methane. This suggest that CO dissociation is significantly hindered.

3.3.3. Catalytic investigations at sub-atmospheric pressure in a closed loop circulation reactor using $^{13}CO_2$.

Our closed loop circulation system (shown in Fig. 2) working at sub-atmospheric pressure allows us to follow the interconversion of carbon atoms of both reactants, because one of the reactants is labeled ($^{13}CO_2$). Note that in this case the temperature programmed DRM reactions were conducted with stoichiometric ratio of the reactants (~25 mbar CH_4 + ~25 mbar labeled $^{13}CO_2$). (CH_4 reactant contained 2% Ar for internal reference of mass signal changes due to the pressure and temperature increase during the experiment.) The dry reforming reactions were always preceded by a reduction at 600 °C in atmospheric H_2 flow and evacuation. Two types of experiments were carried out in this system: ramp-hold and isothermal tests. The first consisted of a temperature ramp from about

100 ºC up to 600 °C followed by a 30 min isothermal hold, evacuation of the gas phase, then cooling. Although quantitative analysis (exact concentrations) cannot be obtained here due to the significant pressure increase during reaction, comparison of the experimental curves normalized to Ar signal (m/e=40) can still provide comparable information about the catalysts. As it is seen in Fig. 16 a-d, the reaction starts at around 300 ºC, and products such as ^{13}CO, ^{12}CO and H_2 are formed and with a low concentration $^{12}CO_2$ and $^{13}CH_4$ are detected at different temperatures depending on the catalyst. As Fig. 16 d shows, first ^{13}CO originating from carbon dioxide reactant can be observed on all samples. The ^{12}CO coming from methane appears at very similar time/temperature like $^{12}CO_2$ and H_2 on the Zr6Ni3_iw and Zr8Ni1_sol, while in the case of the Na_2O-promoted samples the $^{12}CO_2$ and H_2 formation precedes by at least 30 °C the ^{12}CO appearance. This suggests that at the onset of methane dissociation (sharp increase of H_2 signal intensity), the available oxygen species are in excess and can make total oxidation of ^{12}C on the promoted samples. The $^{12}CO_2$ formation has always a local maximum, afterwards, it is consumed together with the labeled $^{13}CO_2$ as the temperature increases. Johnson and Shamsi[61] also observed during $^{13}CH_4$ labeled flow dry reforming experiments the formation of $^{13}CO_2$ at 800 ºC.

Eye-catching is the evolution of labeled $^{13}CH_4$ (m/e=17) on Zr8Ni1_sol (Fig.16 a) and Zr6Ni3_iw (Fig. 16 c) at relatively low temperatures. The effective hydrogenation of carbonates leading to formates under dry reforming conditions on these catalysts produces finally methane in the appropriate temperature and concentration window from $H^{13}COO_s$ /$^{13}CHO_s$/$^{13}C_s$. Furthermore, methanation proceeds on metallic Ni sites and it is structure sensitive reaction, and sensitive to the presence of H_2 that induces CO dissociation.[62] However, dissociation of CO is inhibited by O traces.[63]

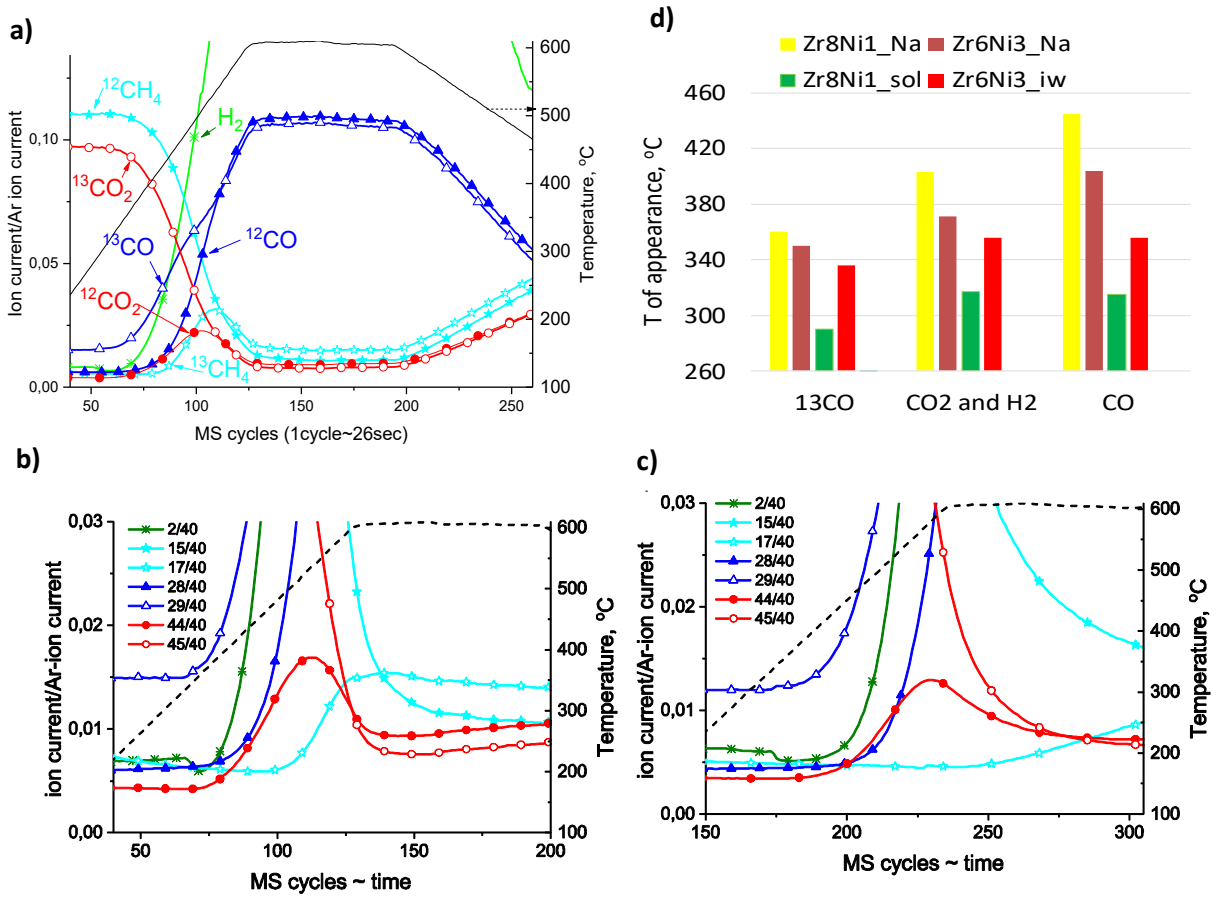

Fig. 16. Ramp-hold type dry reforming reaction with $^{13}CO_2$:$^{12}CH_4$=1 mixture in the closed loop circulation system on a) Zr8Ni1_sol, b) Zr6Ni3_iw (enlarged), c) Zr6Ni3_Na (enlarged) and d) Temperature of products' appearance on all the investigated samples. (^{13}CO m/e= 29, ^{12}CO m/e=28, H_2 m/e=2, $^{12}CH_4$ m/e=15 and $^{13}CO_2$ m/e=45, Ar m/e=40).

In the case of the promoted Zr6Ni3_Na (Fig. 16 c), the $^{13}CH_4$ formation is retarded until the shortage of oxygen/oxidants (from CO_2), although abundant H_2 is available, while labeled methane is not formed at all on Zr8Ni1_Na. Arena et al.[43] reported that surface diffusion of hydrogen is hindered by alkali patches on Ni. This might be also valid for the present case, further depressing the methanation route. Although we could not go higher than 500 °C during DRIFTS measurements, we suppose that some short lived carbonates are present even at 600 °C due to the Na_2O promoter around $Ni/Ni(OH)_2$, and by a continuous formation and decomposition they provide oxygen to $^{12}C_xH_y$ or C_s removal. Indeed, HRTEM investigation of Zr6Ni3_Na showed a Ni particle decorated with $Ni(OH)_2$ and NiOOH patches after this ramp-hold experiment.

TPO measurement after these ramp-hold reactions revealed different type and amount of deposited coke on the samples. For a clearer view, the integral signal of CO_2 formation obtained in the closed loop circulation system was differentiated. On Zr6Ni3_iw (Figure 17 a) and on Zr8Ni1_sol (not shown here) surface carbon originating from $^{12}CH_4$ source was oxidized at around 330 °C with a significant tail at 520 °C or a distinct peak at 550 °C for Zr8Ni1_sol. At the higher temperature range $^{13}CO_2$ was also detected on both samples, meaning that the less reactive carbon deposit was a mixed type (from both ^{12}C and ^{13}C). This means that methane leaves an easily oxidizable (low temperature TPO peak) carbon and a more resistant type of carbon (high temperature tail) on Ni/ZrO_2, moreover, a "mixed type" coke partly from gas phase ^{12}CO and ^{13}CO product is also formed. In contrast to this, on Zr6Ni3_Na only ^{12}C was remained with a wide reactivity/distribution. The detailed quantification of ^{12}C and ^{13}C ratio of the total deposited carbon on two chosen catalysts and under both type of reactions (ramp-hold and isothermal) are collected in Table 3. This analysis helps to distinguish the contribution of the CO_2 activation route to the inactive carbon formation for each catalyst and conditions as it was done in refs[23,24,25] . It is seen in Table 3 that the amount of deposited carbon was drastically decreased upon sodium promotion, while the contribution of CO_2 to the total carbon is similarly low (only 10% on Zr6Ni3_iw, and zero on the promoted catalyst) in the ramp-hold experiments.

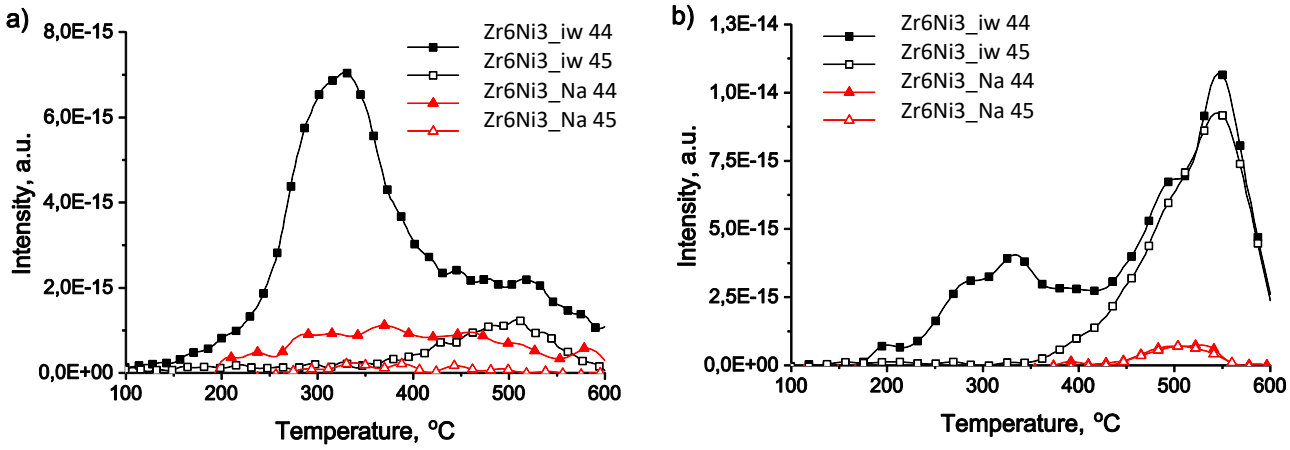

Fig. 17. TPO experiments in circulation system after labeled DRM reaction carried out via a) ramp-hold manner and b) isothermal manner at 600 °C on two chosen samples. $^{12}CO_2$: full symbols, $^{13}CO_2$: empty symbols. The original measured integral signals are differentiated to get peak-shaped curves.

The other dry reforming experiments carried out in the circulation system were of isothermal type (600 °C reaction for 30 min then evacuation of the gas phase, cooling). These results are not shown here, but by the end of 30 min reaction time, practically all the reactants were converted, and the low concentration components right after the start of the reaction showed exactly the same profile in Figure 16 b and c: $^{12}CO_2$ immediately formed then consumed, while $^{13}CH_4$ was detected within 1 or after 4.5 min on Zr6Ni3_iw and Zr6Ni3_Na respectively. The tendentious decrease of

both CO products and the increase of CO_2 signals on Zr6Ni3_iw suggested that CO disproportionation happened at 600 °C leaving some C_s on Ni. In contrast, methane conversion was relatively slow on Zr6Ni3_Na, and based on the less amount of H_2 evolved compared to that on Zr6Ni3_iw, we assume that H_s/OH_s species remained on the catalyst.

Table 3. Quantified results of TPO experiments in circulation system after labeled DRM reactions carried out via the ramp-hold or the isothermal manner at 600 °C.

Sample	T/°C and type of exp.	$^{12}CO_2$ /μmol*g^{-1}	$^{13}CO_2$ /μmol*g^{-1}	$^{12}C/^{13}C$	Total C /μmol*g^{-1}
Zr6Ni3_iw	600, ramp & hold	1425.9	159.2	8.95 (10)[a]	1585.1 (1.92)[b]
	600, isothermal	1030.8	647.6	1.59 (38.6)[a]	1678.3 (2.08)[b]
Zr6Ni3_Na	600, ramp & hold	250.0	0.0	n/a (0)[a]	250.0 (0.3)[b]
	600, isothermal	46.3	38.0	1.22 (45.1)[a]	84.4 (0.11)[b]

[a] % contribution of the CO_2 activation route to the total surface carbon derived from both CH_4 and CO_2 activation routes
[b] wt% carbon

The corresponding differentiated TPO curves are shown in Fig. 17 b. On Zr6Ni3_iw about the same amount of coke formed as in the ramp-hold experiment but the CO_2 contribution increased now to about 38.6% (Table 3). We propose that the high temperature peaks on Zr6Ni3_iw were formed from the CO products via the Boudouard-reaction (2 CO⇌C+CO_2) and from $^{12}CH_4$ at the start of the reaction. The active sites for CO dissociation on this sample seem to be more effective/available during the isothermal experiment than during the ramp-hold type one, because they might be less covered by carbon deposits originating solely from CH_4 decomposition (see the area of the low temperature peak). This again justifies the general view that at higher temperature less carbon deposit is expected to form. In the case of Zr6Ni3_Na, we observed now the presence of carbon from the $^{13}CO_2$ reactant which was not the case during the ramp-hold type experiments: the even more negligible surface carbon was a "mixed type" with 45% contribution of ^{13}C. This deposited carbon is assumed to originate either from CO products, or may show that the CH_4 and CO_2 activation routes produce surface carbon with the same structural characteristics[25].

In general, we can observe that the contribution of $^{13}CO_2$ in the deposited coke is increased during the isothermal experiments for both samples, when the reaction starts /proceeds faster. Note the main difference: coke did not form on the promoted sample solely from CH_4 reactant as opposed to Zr6Ni3_iw under the same type isothermal reaction. This means that localized Na promotion helps the gasification of a reactive surface – probably CH_x type – carbon in a continuous and effective way via the embedded Na_2O entities forming carbonates and acting according to the reverse of Boudouard reaction: $CH_x + CO_2 \rightleftharpoons 2\ CO + x\ H_s$.

3.3.4. The role of sodium promotion in the reaction mechanism and coke removal

Connecting catalytic properties with all the structural results, we can draw the following statements. The highly hydrated iw catalysts active in formate production under low temperature dry reforming conditions will develop deactivating type coke. Formate formation stems from the metal surface providing H_s, thus part of that formate must be in the surrounding of Ni particles occupying/poisoning adsorption area from CO_2 reactant that could provide new active oxygen species to C_s removal. At high temperature, when the interface of Ni might not play significant role in CO_2 activation, but the metal surface itself, CO disproportionation must be avoided in order to get stable catalytic performance.

On Na-promoted samples formate was not observed – due to its complete absence or immediate decomposition to carbonates – the dry reforming ability was preserved without significant deactivation. In this case the localized Na_2O-promotion on and around the $Ni/Ni(OH)_2$ entities is of key importance that can be achieved when sodium is added at the same time as Ni precursor during preparation. Even though the existence of a bridged CO species at 1820 cm^{-1} suggests a decreased C-O bond strength, increased CO dissociation ability was not deducted on the promoted samples. The stable activity under our real demanding dry reforming conditions is explained by the continuously renewing oxygen pool from the balanced interconversion of $NaHCO_3/Na_2CO_3/Na_2O$ at the Ni-ZrO_2 interface or partially on the surface of Ni particle. Ni – through dissociation of CH_4 – provides H_s to the decomposition of Na_2CO_3 or $NaHCO_3$ to $CO_2+O^{2-}+ Na^+ + H_2O$. During the process NiO_xH_y forms that is reduced by C_s or C_xH_y (from methane) back to Ni (and CO and H_2O forms). Then Na_2O and the available CO_2 results in Na_2CO_3 again. These tentatively suggested reactions take place simultaneously on small domains of Ni surface or at the interface. Metallic Ni part is required for CH_4 dissociation, $Ni(OH)_2$ or NiOOH (NiO_xH_y) for carbon oxidation. Our assumption is strongly supported by literature references[45,46,64] reporting about high CO_2 absorption capacity of bulk Na_2ZrO_3 in the presence of CO_2 at temperatures above 500 °C resulting Na_2CO_3 shell and ZrO_2 layer beneath close to the surface of bulk alkali zirconate as:

$Na_2ZrO_3 \rightarrow ZrO_2+O^{2-}+2Na^+$ (3)

$CO_2+O^{2-}+2Na^+ \rightarrow Na_2CO_3$ (4).

At higher temperature (~800-850 °C) or at lower CO_2 partial pressure the Na_2ZrO_3 is regenerated by CO_2 liberation forming Na_2O that can react with ZrO_2 producing Na_2ZrO_3 again (the reverse directions of reactions (3) and (4).[45, 46, 64] We propose that the upwards diffusion of sodium ions in the surface labile oxide lattice to capture CO_2 could result that some O^{2-} species are used up by C_s. This must have multiple relevance at high reaction temperatures of our long term catalytic tests. Until there is a small amount of gas phase CO_2, the "primary" carbon of methane reactant is removed and not deposited as coke neither hydrogenated back to CH_4.

4. Pt and NiPt catalysts

As noble metals do not form carbide phase, coke formation on Pt was expected to be low. Due to financial reasons, Pt consumption must be omitted or reduced as low as possible. In this short section, two monometallic Pt and three bimetallic NiPt catalyst with or without sodium addition and a sol-derived one are discussed (see Table 1 for details). With the variation of preparation methods of the bimetallic samples the degree of alloying was to be changed.

4.1. Structural characterization of the Pt, NiPt catalysts: dispersion, XPS, XRD, TEM, TPR, DRIFTS (CO chemisorption and DRIFTS-DRM reaction)

Dispersion data (by CO pulse chemisorption) and H_2 consumption are seen in Table 4 and TPR curves are shown in Fig. 18. H_2 consumptions are determined after low temperature (mild TPR) calcinations on the Pt samples, because after calcination at 700 °C the platinum oxide decomposed to Pt and so there was no oxide to reduce in the subsequent TPR run (and Pt sintered a lot). The sodium-promoted Pt was easier to oxidize than the unpromoted one: Pt(IV) was reduced on Zr8Pt1_Na after calcination at 400 °C (TPR peak at 160 °C), while 600 °C was needed to oxidize platinum on the iw sample to Pt(II) on Zr8Pt1_iw (TPR peak at 120 °C).

The possibility of Pt-oxide decomposition after 700 °C calcination makes the reducibility calculation of the bimetallic catalysts more complicated (here always 700 °C calcination was used prior to the TPR run). If we assume 100 % Pt-oxide decomposition, Ni(II) content would give 7.64 cm^3/g_{cat} H_2 consumption. Anything above this H_2 consumption can be explained by the different oxidation states of the metals. Below this minimum H_2 consumption is that of the sol sample's – it is surprising as this suggests a Ni oxidation state lower than 2+ or the presence of NiO_xH_y sites that

cannot be reduced at all (presence of $B_xO_yH_z$?), although, XPS did not detect only minute Ni^{2+} in this sample.

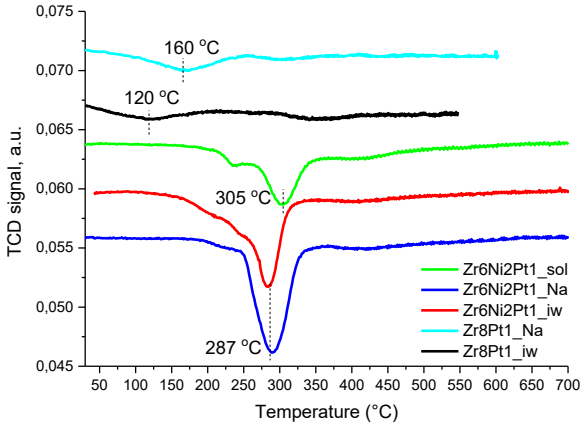

Fig. 18. TPR curves of Pt and NiPt catalysts

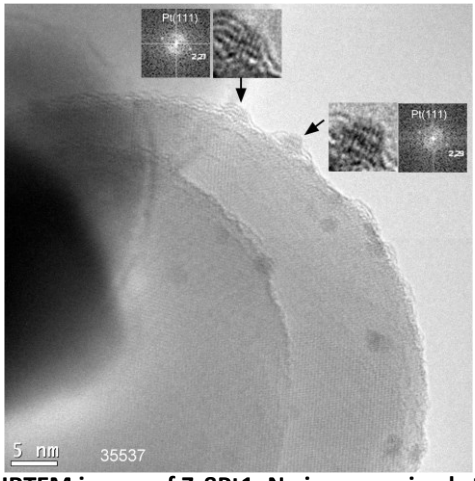

Fig. 19. HRTEM image of Zr8Pt1_Na in as received state

As for metal dispersion (Table 4), note the similarly high dispersion of Pt as expected in a supported noble metal catalyst at low loading on both samples (Fig. 19 shows Zr8Pt1_Na). Among the bimetallic catalysts the sodium-promoted sample adsorbed the least CO, but again, this might be the electronic and steric effect of Na_2O as in the case of Ni samples. XRD of the bimetallic samples reflected a higher degree of alloying in the following order: iw < Na < sol sample (see Table 4). The repeated calcination/reduction cycles (TPR experiments) increased the alloying of Ni and Pt. As the XRD peaks were of very low intensity (see for example Fig. 20), the results should be taken with some consideration, however, according to these results iw method cannot ensure a good mixing of Ni and Pt precursor, while in the two other samples the degree of alloying riches or even increases the theoretical values.

Table 4. Dispersion, TPR and XRD results of Pt and NiPt samples

sample name	metal dispersion by CO pulse chemisorption	H_2 consumption during TPR cm^3/g_{cat}	Pt substitution by XRD, % (theoretical: 13)	
			as received	after TPR
Zr8Pt1_iw	16.2 %	1.2		
Zr8Pt1_Na	18.9 %	1.9		
Zr6Ni2Pt1_iw	1.85 %	8.78	0	4
Zr6Ni2Pt1_Na	0.86%	9.15	8	22
Zr6Ni2Pt1_sol	3.36 %	6.85	40[a]	40

a: 24 % by HRTEM

XPS measurements carried out on Zr8Pt1_Na showed a negative BE shift for Pt in the reduced state that suggest that strong (electronic) interaction persist in reducing atmosphere between small platinum nanoparticles and the support containing alkali ions (Pt nanoparticles covered with ZrO_x or even with Na_2O patches?). Among the bimetallic samples, Zr6Ni2Pt1_sol was only measured by XPS: the presence of metallic Ni was seen after in situ reduction as Fig. 21 depicts. The surface Pt/Ni ratio increased after in situ reduction that suggests the surface enrichment of Pt in Zr6Ni2Pt1_sol. (The theoretical Pt/Ni_{bulk}=0.15 was measured in the as received state of this sample).

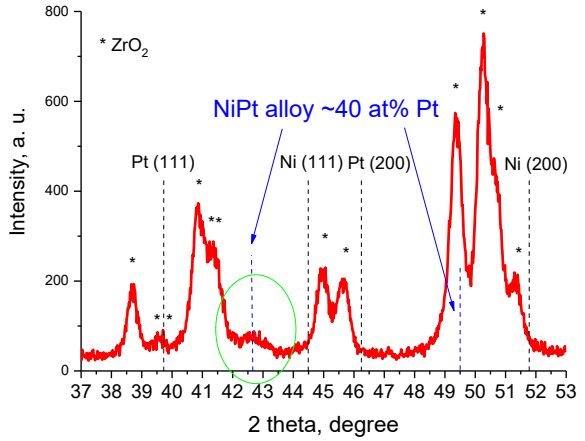

Fig. 20. XRD pattern of Zr6Ni2Pt1_sol in as received state

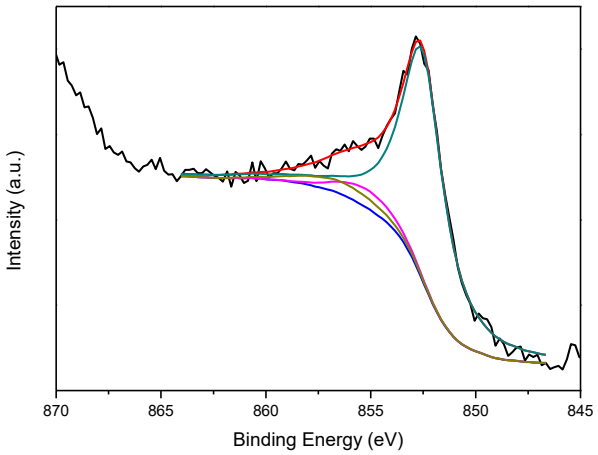

Fig. 21. XPS spectrum of Ni $2p_{3/2}$ region of Zr6Ni2Pt1_sol after in situ calcination/reduction at 600°C

CO TPD after CO pulse chemisorption was again followed by QMS. It is interesting to highlight that CO was not observed at higher temperatures on the Na_2O promoted-samples in contrast to the rest of the samples (see Fig. 22). Again, the somewhat higher basicity of the promoted catalysts is reflected in the high temperature of CO_2 peaks. As for the Pt catalysts, the dispersed samples produced H_2 peak around 200 °C (the sodium-promoted produced solely this peak), while after 700 °C calcination and reduction (low dispersion) resulted in no more such H_2 peak (Fig. 22, left side, middle spectrum). As for the bimetallic samples, the H_2 peak(s) appear at the lowest temperature on the sodium promoted sample (at 190 and 288 °C) and the ratio of H_2/H_2O intensity is the highest on the sol-derived catalyst. We tentatively propose that this H_2 is produced on the metal or at the metal-support interface.

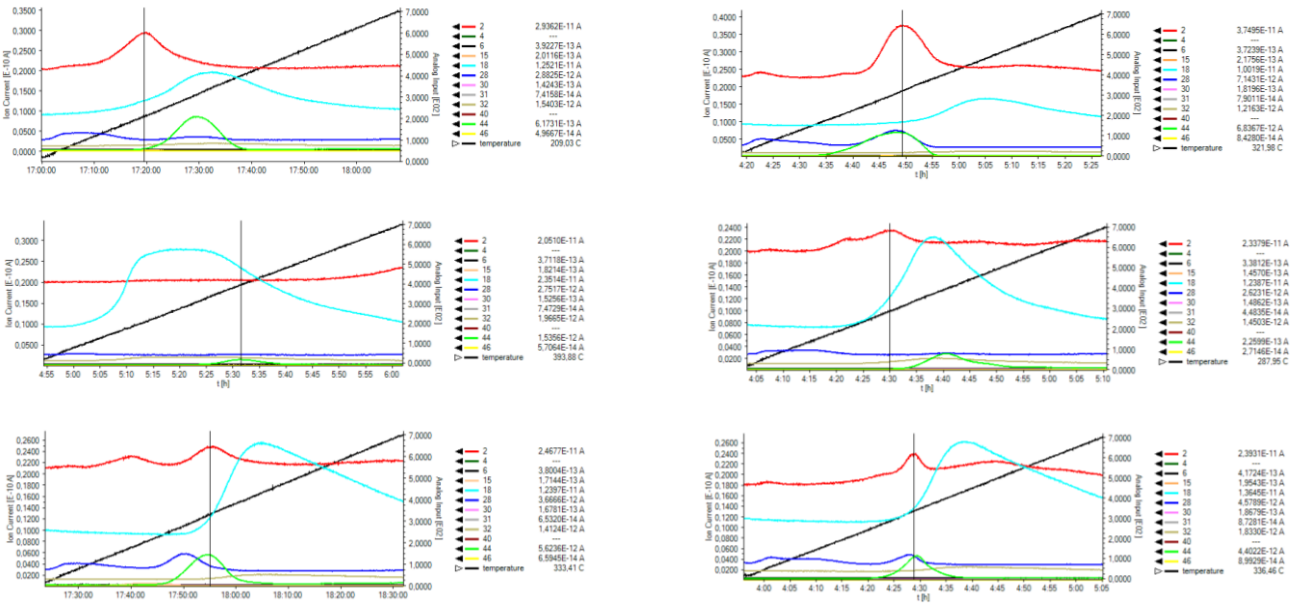

Fig. 22. CO TPD spectra after CO pulse chemisorption in He. Left side from top to down: Zr8Pt1_Na after mild TPR, Z8Pt1_Na after normal TPR, Zr8Pt1_iw after mild TPR. Right side from top to down: Zr6Ni2Pt1_sol, Zr6Ni2Pt1_Na, Zr6Ni2Pt1_iw (red curves: H_2, light blue: H_2O, green: CO_2, dark blue: CO)

CO chemisorption at room temperature was studied by DRIFTS as is shown in Fig. 23. The linear CO bond to metal sites is located at the same position (2083 cm^{-1}) on all samples. The very intense linear CO bands show that the surface of the bimetallic particles is Pt-dominated. The distinct shoulders at around 1940 cm-1 assigned to the bridged bond CO on the bimetallic samples reflects the presence of Ni or NiPt surface. Note, that CO connected to the acidic sites of ZrO_2 support (2184, 2194 cm^{-1}) is detected only on the iw samples. And finally, the special band at around 1804 cm^{-1} of the Na-promoted samples is again observable.

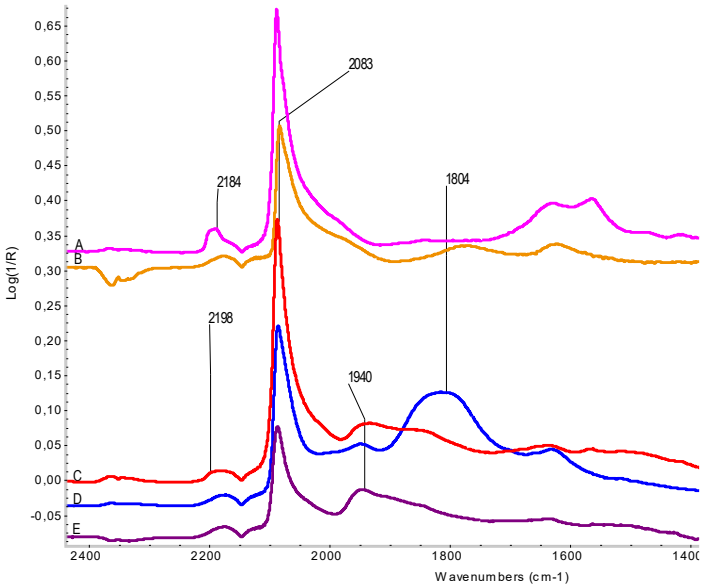

Fig. 23. DRIFTS spectra in 1%CO/He at 25 °C on A) Zr8Pt1_iw, B) Zr8Pt1_Na, C) Zr6Ni2Pt1_iw, D) Zr6Ni2Pt1_Na, E) Zr6Ni2Pt1_sol

DRIFTS measurements in the presence of DRM mixture flow was carried out as in the case of Ni samples. Fig. 24 depicts the results obtained at the lowest and the highest temperatures.

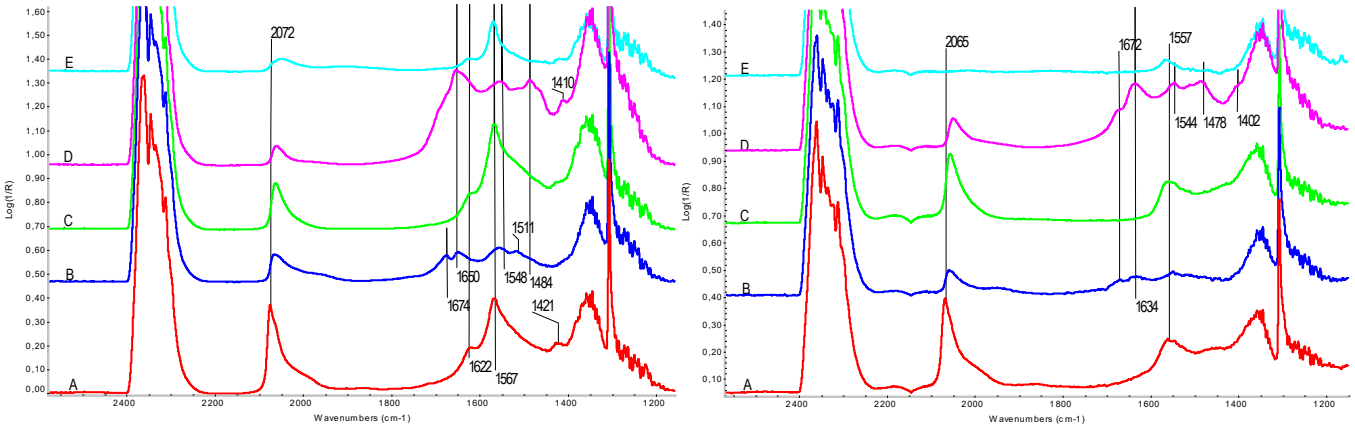

Fig. 24. DRIFTS spectra obtained in the presence of CH_4:CO_2=70:30 DRM flow at left) 300 °C and right) 500 °C. Curves: A) Zr8Pt1_iw, B) Zr8Pt1_Na, C) Zr6Ni2Pt1_iw, D) Zr6Ni2Pt1_Na, E) Zr6Ni2Pt1_sol

During the reaction, the highest intensity of CO bond to metal is seen in the case of the iw samples (Curves A and C) while it is the lowest for Zr6Ni2Pt1_sol (showing that more Ni is alloyed with Pt). The carbonate region of the spectra resembles those of the corresponding monometallic Ni catalysts' again: Na_2O promotion produces bridged bidentate and monodentate carbonates at 1674, 1650, 1548 cm^{-1} and some carboxylates/polydentate carbonates at 1511, 1484, 1410 cm^{-1}. The main difference that on monometallic Pt catalyst the intensity of carbonates is really low already at 300 °C, while for the bimetallic Zr6Ni2Pt1_Na

sample the bands are more intense. This may suggest that the nicely dispersed small Pt particles play a role in the destabilization/conversion of carbonates formed on the Na_2O-ZrO_2 and the bimetallic particles are less efficient in doing so (obviously metal dispersion must be lower, see Table 4). On the samples without Na, bicarbonates and at 500 ºC mainly formates are detected (1622, 1421, 1567 cm^{-1}), and their intensity does not depend on the type of metals for the mono or bimetallic iw samples, (curves A and C). There is a less intense formate band on Zr6Ni2Pt1_sol reflecting that the support is not really efficient in CO_2 adsorption/activation (acidic).

4.2. Catalyst stability and coke formation in fixed bed reactor

Finally, the catalytic stability tests will be shortly discussed. As Pt is not able to form bulk carbide, coke formation on the monometallic Pt samples was expected to be low even under our severe conditions (excess of CH_4). Fig. 25 depicts the conversion curves obtained together with the results of the subsequent TPO measurements. It seems that Na_2O promotion does not influence the methane conversion, but a little higher CO_2 conversion and the absence of carbon deposits is observed compared to Zr8Pt1_iw. Thus, it seems that sodium-promotion in the case of Pt catalysts plays a role in hindering inactive carbon formation (as in the case of nickel catalysts) but the activity of Pt is not changed.

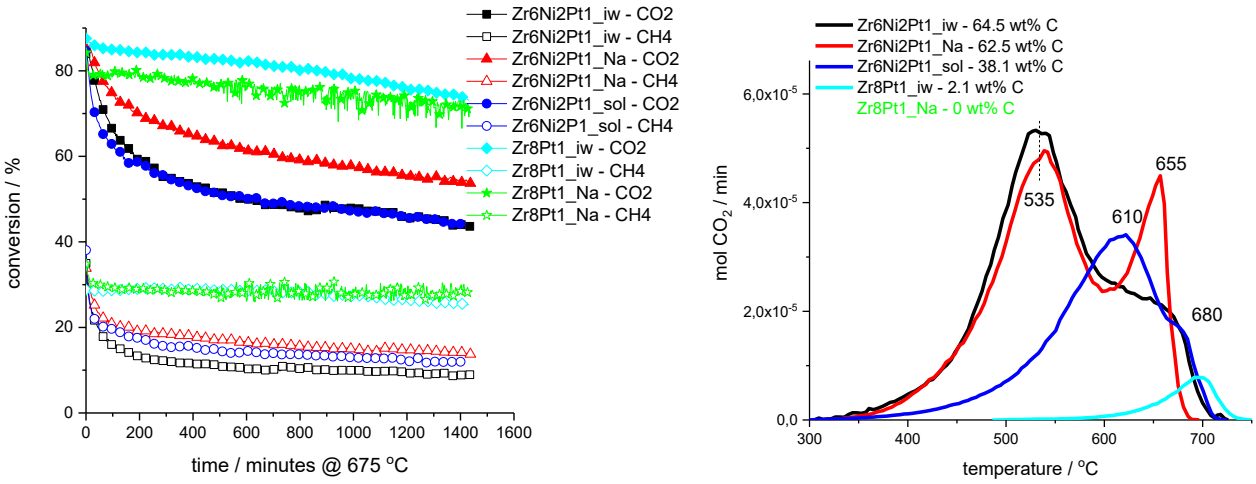

Fig. 25. Methane and CO_2 conversion curves during long term stability run at 675 ºC on monometallic Pt and bimetallic NiPt samples (left side) and the corresponding TPO curves with wt% carbon content (right side). Note that catalyst weight for Pt samples: 30 mg, for bimetallic samples: 15 mg.

As for the bimetallic catalysts, we can directly compare the conversion values with those measured on the monometallic Ni samples, since the moles of Ni in the reactor was the same. The best catalytic performance was attained on Zr6Ni2Pt1_Na, and again, the CO_2 conversion was the highest as well. It is somewhat unpredicted that alloying Ni with Pt does not change or enhance the catalytic activity, stability in the case of sodium promotion, neither in the case of sol synthesis route, while it greatly improves in the case of iw preparation method. Moreover, on all bimetallic catalyst the carbon formation is increased compared to the monometallic Ni counterparts (see TPO data). The effect of Na_2O-promotion in carbon removal during the TPO run is reflected in the different oxidation kinetics of deposited coke removable at 655 ºC (see the sharp peak) compared to the rest of the samples. We speculate that the localization of Na_2O promotor entities must be different than in the case of Zr6Ni3_Na. Furthermore, the bimetallic particles as they are easier to reduce, stay full metallic and accumulate more carbon from CH_4 decomposition (no possibility of NiO_xH_y formation during the reaction). This assumption will be proved or denied by XPS measurements in the near future.

All in all, we succeeded to produce by the localized Na_2O promotion of the Ni-ZrO_2 system a catalyst that is similarly active and stable as the expensive Pt reference sample. The coking tendency can be tuned by the Ni loading in the expense of catalytic activity.

5. Ni-In/SiO_2 system as future possibility for coke-free dry reforming

Beside the above well-detailed studies we started working with indium as a possible modifier. This area turned out to be very promising and the results deserved a separate OTKA research work led by Ferenc Somodi. However, all the technical and some of the theoretical background stem from the present parent project. Shortly, it was shown that the presence of 2 wt% indium on the surface of a 3wt%Ni/SiO_2 catalyst prevented coke formation during dry reforming of methane. The presence of indium profoundly changed the adsorption properties of nickel, as CO-TPD measurements suggested. XPS measurements showed changes in the electronic structure of nickel after reduction and an indium enrichment on the surface. In parallel with this, HRTEM analysis of the bimetallic catalyst showed the presence of NiIn and Ni_2In alloy nanoparticles. The higher catalytic activity and outstanding carbon tolerance of the bimetallic Ni-In/SiO_2 catalyst was explained with the structural and electronic effects of indium.

6. Final conclusions

In the present project we succeeded to accomplish the following main tasks: 1) development of highly active and stable, noble metal-free Ni catalysts that work under realistic conditions using a model biogas, 2) investigation of the reaction steps with labeled reactants and 3) determination of the coke structure and its formation routes on each catalyst system and finally, 4) building new experimental setups that allow the in-depth characterization to provide feedback for the next catalyst generation.

Traditional impregnation, modified wet impregnation and sol-based preparation methods were applied to get Pt, Ni and bimetallic PtNi/ZrO_2 catalysts aiming to decrease the unwanted coke formation during the reaction. The sol-based route was chosen to decrease the particle size via the fast aqueous reduction of metal precursors and to efficiently alloy Pt and Ni in the bimetallic samples. The effect of sodium promotion on the properties of ZrO_2 supported Ni dry reforming catalysts was deeply characterized, which is not widely studied in the literature. Sodium was introduced prior to or simultaneously (Na-Ni/ZrO_2) with the metal precursor.

The most important outcome of the present research project was that adding minute 0.6 wt% Na_2O to Ni/ZrO_2 catalyst in a controlled way a very effective dry reforming catalyst can be attained. The localized Na-incorporation provided high basicity to the catalyst and resulted in a NiO_xH_y that is in strong interaction with the support compared to the reference. Na was enriched on the surface and the inclusion of some sodium oxide into the nickel (oxide) phase was suggested to happen and/or Ni surface became covered by Na_2O or Na_2CO_3 patches based on XPS results and the depressed CO chemisorption values. CO TPD results suggested low temperature WGSR activity signed with H_2 development below 200 ºC, which predicts a non-deactivating catalytic behavior. DRIFTS measurement under flow of the dry reforming mixture revealed the presence of bidentate formate species on Ni/ZrO_2, while no sign of formates was discerned on Na-Ni/ZrO_2. This is because under the reaction conditions they immediately transform to carbonates due to the presence of active surface oxygen or OH species. The rate of this transformation is influenced by the location of Na that is determined by the preparation method. The continuous flow catalytic tests in excess methane revealed different degree of coke deposition, but the activity and stability of Na-Ni/ZrO_2 samples were significantly higher. TPO experiments proved that the surface carbon on the promoted catalyst was a mobile and reactive type one and did not cause significant deactivation. $^{13}CO_2$ labeled stoichiometric DRM experiments were conducted in a closed loop circulation system at sub-atmospheric pressure. Here, evolution of labeled $^{13}CH_4$ was detected on the unpromoted Ni/ZrO_2 due to its effective hydrogenation activity and the dissociation of ^{13}CO on Ni. In the case of the promoted catalyst, this methanation (transfer of ^{13}C of $^{13}CO_2$ to $^{13}CH_4$) was retarded until the

significant shortage of oxygen/oxidants, although abundant H_2 was available. The same was ascertained in our preliminary SSITKA experiments, however, residence time of intermediates leading to CO product was found double on the promoted catalyst. Under isotope labeled dry reforming reaction at 600 ºC, carbonaceous deposit did not form on Na-Ni/ZrO_2 solely from CH_4 reactant in opposite to the base Ni/ZrO_2. This type of coke deposition was thought to be responsible for catalyst deactivation. As for the reaction mechanism in the Na-Ni/ZrO_2 system, we suppose that some short lived carbonates/hydrocarbonates are present even at high temperatures in contact with ZrO_2-embedded Na_2O and Ni/$Ni(OH)_2$ surface, continuously forming and decomposing, thus oxidizing the $^{12}C_xH_y$ or C surface species to ^{12}CO. Thus, the high temperature reversible CO_2 capture of bulk Na_2ZrO_3 cited in the literature is highly exploited here at nanoscale, if the concentration of Na_2O-ZrO_2-Ni/NiO_xH_y domains is maximized (preparation by simultaneous sodium promotion). Note, that the coking tendency can be tuned by the Ni loading in the expense of catalytic activity. Concerning all the results, carbonates on Na-Ni/ZrO_2 are suggested to take part in the reaction while on Ni/ZrO_2 the formates are only spectators in the course of low temperature dry reforming.

The effect of sodium in the case of a well dispersed Pt/ZrO_2 catalyst played a role in hindering inactive carbon formation (as in the case of nickel catalysts), but the activity of Pt was not changed.

As for the bimetallic systems, it was observed that alloying Ni with ~ 15 % Pt did not change the catalytic activity in the case of sodium promotion, neither in the case of sol synthesis route, while it greatly improved in the case of incipient wetness preparation method. Moreover, on all bimetallic catalysts the inactive carbon formation was increased compared to the monometallic Ni counterparts. We speculate that the localization of Na_2O promotor entities must be different and/or the bimetallic particles as they are easier to reduce, stay full metallic and accumulate more carbon from CH_4 decomposition (no possibility of NiO_xH_y formation during the reaction).

The ease of sample preparation and the good properties of the resulting Na_2O-modified catalyst deserves attention and may propagate further research on carbon resistance of Ni supported on non-reducible ZrO_2.

Supplementary notes

As it is seen, a great amount of research work has been done during the project. Those above are only the most important results. However, it is clear that the publication activity legs behind. About half of the results on Ni samples and most of them on Pt and NiPt catalysts have not been published yet. This is due to the fact that well-experienced participants who had the capability of manuscripts writing became retired or unfortunately died. The new project leader had unforeseen duties because of the reconstruction of the academic institution. Moreover, the young colleagues enrolled to the department and got engaged with dry reforming had to be taught to handle the instruments, prepare catalysts and gain some basic knowledge of the topic. Unfortunately, one of the new hires left in the middle of the project unexpectedly, which also slowed down the progress of the research. Furthermore, the new techniques introduced during this time period had to be planned, purchased and constructed (AutoChem, vacuum-DRIFTS cell, circulation system with isotope labeling, SSITKA, etc). These all led to good quality but not as many as expected published papers. However, as the interpretation of the results is at hand now, supposedly 3 manuscripts will be submitted in the near future.

References

1 P. M. Mortensen and I. Dybkjaer, *Appl. Catal. A: Gen*., 2015, **495**, 141.
2 M. K. Nikoo and N. A. S. Amin, *Fuel Proc. Techn*., 2011, **92**, 678.

[3] A. Yamaguchi and E. Iglesia, *J. Catal.*, 2010, **274**, 52.
[4] J. Wei and E. Iglesia, *J. Catal.*, 2004, **224,** 370.
[5] N. Sun, X. Wen, F. Wang, W. Peng, N. Zhao, F. Xiao, W. Wei, Y. Sun and J. Kang, *Appl. Surf. Sci.*, 2011, **257,** 9169.
[6] B.B. Baeza, C.M. Pedrero, M.A. Soria, A.G. Ruiz, U. Rodemerck, and I.R. Ramos, *Appl. Catal. B: Environ.*, 2013, **129,** 450.
[7] S. Sokolov, E.V. Kondratenko, M.M. Pohl and U. Rodemerck, *Int. J. Hydrogen Energy*, 2013, **38,** 16121.
[8] S. Damyanova, B. Pawelec, K. Arishtirova, M.V.M. Huerta and J.L.G. Fierro, Appl. Catal. B: Environ., 2009**, 89,** 149.
[9] A.S. Bobin, V.A. Sadykov, V.A. Rogov, N.V. Mezentseva, G.M. Alikina, E.M. Sadovskaya, T.S. Glazneva, N.N. Sazonova, M.Y. Smirnova, S.A. Veniaminov, C. Mirodatos, V. Galvitta, and G.B. Martin, *Top. Catal.*, 2013, **56,** 958.
[10] L.M. Aparicio, *J. Catal.*, 1997, **165,** 262.
[11] M.C.J. Bradford and M.A. Vannice, *J. Catal.*, 1998, **173,** 157.
[12] Y.Z. Chen, B.J. Liaw, and W.H. Lai, *Appl. Catal. A: Gen.*, 2002, **230,** 73.
[13] M. A. Goula, A. Lemonidou and A.M. Efstathiou, *J. Catal.*, 1996, **161,** 626.
[14] J.-M. Wei, B.-Q. Xu, J.-L. Li, Z.-X. Cheng and Q.-M. Zhu, *Appl. Catal. A: Gen.*, 2000, **196,** 167.
[15] Y. Kathiraser, U. Oemar, E. T. Saw, Z. Li, and S. Kawi, *Chem. Eng. J.*, 2015, **278,** 62.
[16] C. Papadopoulou, H. Matralis, and X. Verykios, in *Catalysis for Alternative Energy Generation*, L. Guczi and A. Erdőhelyi (eds.), Springer Science+Business Media New York 2012, 57-128.
[17] M-S. Fan, A. Z. Abdullah and S. Bhatia, *Chem. Cat. Chem.*, 2009, **1,** 192.
[18] J. W. Han, C. Kim, J. S. Park and H. Lee, *Chem. Sus. Chem.*, 2014, **7**, 451.
[19] A. Horváth, G. Stefler, O. Geszti, A. Kienneman, A. Pietraszek and L. Guczi, *Catal. Today*, 2011, **169,** 102.
[20] E. Lovell, Y. Jiang, J. Scott, F. Wang, Y. Suhardja, M. Chen, J. Huang and R. Amal, *Appl. Catal. A: Gen.*, 2014, **473,** 51.
[21] L.F. Li, C. Xia, C.T. Au and B.S. Liu, *Int. J. Hydrogen Energy*, 2014, **39,** 10927.
[22] C. Gennequin, M. Safariamin, S. Siffert, A. Aboukaïs and E. Abi-Aad, *Catal. Today*, 2011, **176,** 139.
[23] M. M. Makri, M. A. Vasiliades, K. C. Petallidou and A. M. Efstathiou, *Catal. Today*, 2015, **259,** 150.
[24] M. A. Vasiliades, M.M. Makri, P. Djinovic, B. Erjavec, A. Pintar and A.M. Efstathiou, *Appl. Catal. B: Environmental*, 2016, **197**, 168.
[25] M.A. Vasiliades, P. Djinović, L.F. Davlyatova, A. Pintar and A.M. Efstathiou, *Catal. Tod.*, 2017, doi: 10.1016/j.cattod.2017.03.057
[26] A. Horváth, L. Guczi, A. Kocsonya, G. Sáfrán, V. La Parola, L. F. Liotta, G. Pantaleo and A. M. Venezia, *Appl. Catal. A: Gen.*, 2013, **468,** 250.
[27] L. Guczi, Gy. Stefler, O. Geszti, I. Sajó, Z. Pászti, A. Tompos and Z. Schay, *Appl. Catal. A: Gen.*, 2010, **375,** 236.
[28] A. Ballarini, F. Basile, P. Benito, I. Bersani, G. Fornasari, S. de Miguel, S.C.P. Maina, J. Vilella, A. Vaccari and O.A. Scelza, *Appl. Catal. A: Gen.*, 2012, **433-434,** 1.
[29] A.D. Ballarini, S.R. de Miguel, E.L. Jablonski, O.A. Scelza and A.A. Castro, *Catal. Today*, 2005, **107-108,** 481.
[30] M. W. Balakos and S.S.C. Chuang, *Journal of Catalysis*, 1992, **138,** 733.
[31] R. D. Gonzalez and H. Miura, *J. Catal.*, 1982, **77,** 338.
[32] C. Zhang, Y. Li, Y. Wang, H. He, *Environmental Science and Technology*, 2014, **48,** 5816.
[33] T. Horiuchi, K. Sakuma, T. Fukui, Y. Kubo, T. Osaki and T. Mori, *Appl. Catal. A: Gen.*, 1996, **144,** 111.
[34] T. Osaki and T. Mori, *J. Catal.*, 2001, **204,** 89.
[35] M. Németh, Z. Schay, D. Srankó, J. Károlyi, Gy. Sáfrán, I. Sajó and A. Horváth, *Appl. Catal. A: Gen*., 2015, **504**, 608.
[36] S. L. Shannon and J. G. Goodwin, *Chem. Rev.* 1995, **95**, 677.
[37] A. Packter and S. C. Uppaladinni, *Kristall und Technik*, 1975, **10** 985.
[38] F. M. Bautista, J. M. Campelo, A. Garcia, D. Luna, J. M. Marinas, M. C. Moreno, A. A. Romero, J. A. Navio and M. Maciasy, *J. Catal*, 1998, **173**, 333.
[39] D. Mazza and M. Vallino, *J. Am. Ceram. Soc*, 1992, **75**, 1929.
[40] J. Ni, L. Chen, J. Lin and S. Kawi, *Nano Energy*, 2012, **1**, 674.
[41] A. Fouskas, M. Kollia, A. Kambolis, Ch. Papadopoulou and H. Matralis, Appl. Catal. A: Gen. 2014, **474**, 125.
[42] F. Arena, A. L. Chuvilin and A. Parmaliana, *J. Phys. Chem.*, 1995, **99**, 990.
[43] F. Arena, F. Frusteri and A. Parmaliana, *Appl. Catal. A: Gen.*, 1999, **187**, 127.
[44] Q. J. Chen, J. Zhang, Q. W. Jin, B. R. Pan, W. B. Kong, T. J. Zhao and Y. H. Sun, *Catal. Today*, 2013, **215**, 251.
[45] H. G. Jo, H. J. Joon, C. H. Lee and K. B. Lee, *Ind. Eng. Chem. Res.*, 2016, **55**, 3833.
[46] G. G. Santillán-Reyes and H. Pfeiffer, *International Journal of Greenhouse Gas Control*, 2011, **5**, 1624.
[47] A. F. Carley, S. D. Jackson, J. N. O'Shea and M. W. Roberts, *Surf. Sci.*, 1999, **440**, 868.
[48] A. Kitla, O. V. Safonova and K. Föttinger, *Catal. Lett.*, 2013, **143**, 517.
[49] P. Panagiotopoulou and D.I. Kondarides, *J. Catal.*, 2008, **260**, 141.
[50] L. F. Liotta, G. A. Martin and G. Deganello, *J. Catal.*, 1996, **164**, 322.
[51] K. I. Hadjiivanov and G. N. Vayssilov, *Adv. Catal.*, 2002, **47**, 307.
[52] J. M. Pigos, C. J. Brooks, G. Jacobs amd B. H. Davis, *Appl. Catal. A: Gen.*, 2007, **319**, 47.
[53] E-M. Kock, M. Kogler, T. Bielz, B. Klotzer and S. Penner, *J. Phys. Chem. C*, 2013, **117**, 17666.
[54] T. Shido and Y. Iwasawa, *J. Catal.*, 1993, **141**, 71.
[55] J. H. Bitter, PhD thesis, *University of Twente, Enschede, the Nederlands*, 1997
[56] S. E. Collins, M. A. Baltanás and A. L. Bonivardi, *J. Phys. Chem. B*, 2006, **110**, 5498.
[57] D. Heyl, U. Rodemerck and U. Bentrup, *ACS Catal.*, 2016, **6**, 6275.
[58] R. W. Stevens, R. V. Siriwardane and J. Logan, *Energy & Fuels*, 2008, **22**, 3070.
[59] T. Shido and Y. Iwasawa, *J. Catal* , 1992, **136**, 493.
[60] Z.-Y. Ma, C. Yang, W. Wei, W.-H. Li and Y.-H. Sun, *J. Mol. Cat. A: Chem*., 2005, **227**, 119.
[61] A. Shamsi and C. D. Johnson, *Catal. Today*, 2003, **84**, 17.
[62] M. P. Andersson, F. Abild-Pedersen, I. N. Remediakis, T. Bligaard, G. Jones, J. Engbæk, O. Lytken, S. Horch, J. H. Nielsen, J. Sehested, J. R. Rostrup-Nielsen and J. K. Nørskov, I. Chorkendorff, *J. Catal.*, 2008, **255**, 6.

[63] S. Fujita, M. Nakamura and T. Doi, N. Takezawa, *Appl. Catal. A: Gen.*, 1993, **104**, 87.
[64] S. Wang, C. An and Q.-H. Zhang, *J. Mater. Chem. A*, 2013, **1**, 3540.